International Forum on Aeroelasticity and Structural Dynamics
IFASD 2017
25-28 June 2017 Como, Italy

VALIDITY OF THE ASSUMPTION OF SMALL DEFORMATIONS IN AIRCRAFT WITH DIFFERENT LEVELS OF STRUCTURAL FLEXIBILITY

Antônio B. Guimarães Neto[1], Flávio J. Silvestre[1], Flávio L. C. Ribeiro[1], Flávio L. S. Bussamra[1], Roberto G. A. da Silva[1], Carlos E. S. Cesnik[2]

[1]Instituto Tecnológico de Aeronáutica
São José dos Campos, SP, 12228-900, Brazil
antoniobgn@gmail.com
flaviojs@ita.br
flaviocr@ita.br
flaviobu@ita.br
gil@ita.br

[2]Department of Aerospace Engineering
University of Michigan, Ann Arbor, Michigan, 48109-2140
cesnik@umich.edu

Keywords: aeroelasticity, flight dynamics, flexible aircraft, small deformations, large deformations

Abstract: A simple and self-contained methodology to assess the validity of the assumption of small deformations in linear structural-dynamic models was recently proposed. The advantages of the methodology lie in the fact that it does not depend on the availability of higher-fidelity, nonlinear models: it is rather based on the selection of two different structural nodes where the structural motion is to be one at a time completely constrained, typically, a node near the center of mass and another in the region of maximum structural displacements with respect to mean axes. If the two displacement vectors calculated in each case can be transformed between themselves with linear rigid-body modes of the structure, then it is still in the regime of small deformations. In the present paper, in order to demonstrate the value of this methodology, it is applied to the X-HALE aircraft in its four-, six- and eight-meter-span configurations, and the results obtained with the assumption of small deformations are compared with a higher-fidelity model that comprises large structural deformations.

1 INTRODUCTION

Recently, a methodology to test for the validity of the assumption of small deformations in linear structural-dynamic flexible aircraft models was proposed and applied to an idealized aircraft model [1]. The methodology is simple and self-contained because it depends only on the linear model itself, not requiring the availability of nonlinear models to compare with.

In structural-dynamic models not to be coupled with aerodynamic counterparts, the methodology is based on the assumption that the linear rigid-body modes of the structural model are representative if, and only if, small deformations occur. Hence, if two different support locations, that is, two different totally-constrained structural nodes are considered, one at a time,

one near the center of mass and the other in the region of maximum deformations with respect to mean axes (in aircraft structures, typically, the wing tips), the conversion of displacement vector from one condition to the other using linear rigid-body modes is possible with minimum error if, and only if, small deformations occur. If there are differences between the original displacement vector and the converted one above some desired tolerance, then large deformations can be assumed to occur and nonlinear models become needed.

If the structural-dynamic model is coupled with an aerodynamic counterpart for aeroelastic or flight-dynamic analyses, then the aerodynamic basis needs to be the same for different structural support locations. In Guimarães Neto et al. [1], this problem was solved with the proposition of an aerodynamic reference frame (ARF) that coexists with the body reference frame (BRF). The latter is the one for which the equations of motion (EOMs) are obtained, with its translations and rotations providing the rigid-body degrees of freedom (DOFs) of the flexible aircraft. The former is the one for which relevant aerodynamic entities, like the angle of attack, the sideslip angle, and aerodynamic angular rates are obtained. A displacement vector with respect to the ARF is also determined, based on the displacement vector calculated for the BRF and a superposition of linear structural rigid-body modes to convert structural displacements from the BRF to the ARF. Hence, if two different structural support locations result in differences in e.g. aerodynamic angle of attack and sideslip angle greater than a desired tolerance, large deformations become the case.

The formulation developed in Ref. [1], however, was obviously not the first dynamically-coupled formulation for the flight dynamics of flexible aircraft. Several works deserve mention for historical and scientific perspective. In this context, the dynamically-coupled formulations are those in which n elastic degrees of freedom are included in the mathematical model of the aircraft, representing its structural dynamics; consequently, the number of flight-dynamic equations of motion (EOMs) increases from the classical six-degree-of-freedom (6-DOF), rigid-body system to an arbitrary 6+n-DOF system.

Bisplinghoff, Ashley and Halfman [7], Bisplinghoff and Ashley [8], and Etkin [9] were among the first to derive dynamically-coupled but inertially-decoupled formulations. However, formulations of this kind would only be used in practical applications more than a decade later due to the necessary development of electronic computing resources. Particularly, from the late 1960s to the middle 1970s, a system of computer programs named FLEXSTAB was developed at the Boeing Company to enable an adequate prediction of the stability characteristics of elastic aircraft at both subsonic and supersonic speeds [10, 11]. The outputs from FLEXSTAB included vehicle deformation and its effects on the trim parameters and the quasi-static stability derivatives [10].

The introduction of n additional structural-dynamic degrees of freedom while keeping the classical six DOFs of the rigid body implies that constraints must be included in the formulations to eliminate the rigid-body DOFs from those of the structural-dynamic model. Such constraints are usually expressed by the choice of body axes. Milne [12] introduced more formalism to this important topic. In his report, three particular choices of body axes were discussed: attached, mean and principal axes.

The origin of the attached axes remains invested in one material point and the axes' directions may be tangent, normal and binormal to a curve of material points that contains the original point [12]. Any set of axes having a fixed orientation with respect to such axes are also attached axes [12]. For the mean axes, the first definition probably arose a few decades before, in 1929

[13]: with respect to them, the linear and angular momenta of the elastic motion are identically zero at every instant. At last, the principal axes are those with respect to which the inertia matrix is diagonal at any instant [12].

In Ref. [1], Milne's concept of attached axes was extended to a more general form named dually-constrained axes, in which the origin of the structural axes (the point where elastic deformations are assumed null) does not necessarily coincide with the origin of the flight-dynamic body axes (with respect to which the EOMs are written). Attached axes became, then, a particular case when such coincidence occurs.

Rodden and Love [14] derived EOMs for a quasi-steady vehicle considering the flexibility matrix derived for the restrained vehicle, but correctly calculating the orientation of the mean axes as a function of the deformation of the restrained structure. Their paper exerted a significant impact on computational aeroelasticity worldwide, since the solution sequence of MSC.Nastran for static aeroelasticity is based on their work [15]. Markedly, the stability derivatives for the restrained aeroelastic aircraft do not depend on the mass distribution, the effects of which are condensed in aerodynamic coefficients dependent upon the inertial accelerations of the vehicle frame [14, 15], a highly-desirable feature in the design of flight simulators. More recently, Dykman and Rodden [16] derived EOMs considering dynamic aeroelastic effects as well, based on the modal superposition technique, and showed that a quasi-steady vehicle formulation can be obtained by the residualization of all modes of vibration.

Considering large rigid-body motions while keeping elastic deformations small, Waszak and Schmidt [17] used Lagrange's equation to derive the same EOMs previously obtained in Refs. [8, 9]. They formalized and used the practical mean-axis constraints and neglected the changes in the inertia tensor due to elastic deformation. A quasi-steady strip-theory aerodynamic model was used to obtain the aerodynamics loads due to the elastic deformation, which in its turn was modeled with a set of normal modes.

Several authors derived formulations that are also readily applicable to finite-element method (FEM) models. References [14] and [16] e.g. can be applied to FEM-modeled aircraft, but they do not consider large rigid-body rotations. Buttrill, Zeiler and Arbuckle [19] derived EOMs considering the availability of a lumped-mass FEM model and retained all the inertial coupling terms. Zeiler and Buttrill [20] refined the EOMs using nonlinear strain-displacement relations to improve the calculation of the incremental stiffness matrix due to nonzero body angular rates – the centrifugal stiffening effect. However, in both studies [19, 20], the rotational DOFs of the lumped mass elements were not considered.

Meirovitch and Tuzcu [21] developed a modular dynamic formulation using Lagrange's equations for quasi-coordinates [22] to derive inertially-coupled, hybrid EOMs. The EOMs were then discretized in space for the solution of the boundary-value problem for the elastic deformation. The authors used a reference frame fixed in the undeformed aircraft. The rotation of the frame and the translation of its origin were treated as the rigid-body DOFs, whereas any displacement relative to the frame was regarded as elastic deformation. The formulation, however, is not easily adaptable to the employment of lumped-mass FEM models with rotational DOFs [23, 24].

Reschke [24,25] also used Lagranges equations for quasi-coordinates in the derivation of EOMs, and had in mind the direct integration with FEM models. Differently from Refs. [19, 20], the author considered the rotational DOFs of the FEM nodes in addition to the translational DOFs.

All inertial coupling terms were derived. The elastic DOFs were represented by free-free modes of vibration, making some but not all of the inertial coupling terms vanish, since no collinearity was assumed between the deformations and the deformation velocities, and variations of the inertia matrix were allowed.

Guimarães Neto [45] derived equations of motion neglecting none of the inertial-coupling terms, and which can be readily applied to aircraft with lumped-mass FEM models. The inertial-coupling terms were however linearized with respect to the structural degrees of freedom, inspired by the method of Hesse and Palacios [28]. Consistent RFAs [49] were used to represent the unsteady aerodynamic effects calculated with the doublet-lattice method [42].

Regarding the formulations for very flexible aircraft, an accident with NASA's Helios Prototype HP03-2 on June 26, 2003 served as an unfortunate demonstration of the importance of adequately modeling the nonlinear behavior of very flexible aircraft. Helios encountered turbulence in flight and morphed into a persistent and unstable high-dihedral configuration that caused an increase in airspeed, which eventually resulted in the wing failure [34]. The investigation board recommended that more advanced, multidisciplinary, time-domain, nonlinear analysis methods should be derived and used for the highly-flexible aircraft [34].

Actually, theoretical work in the field was already being developed at the time. Patil, Hodges and Cesnik [35] developed a nonlinear formulation for the aeroelastic analysis of aircraft in subsonic flow, with a geometrically-exact, nonlinear intrinsic formulation for the beam dynamics in a moving frame [36]. Patil, Hodges and Cesnik [37] extended their work for the flight dynamics of HALE aircraft. Their formulation showed that the trim solution and the flight dynamic modes were directly affected by the wing flexibility. Despite their example aircraft had a straight wing, the trim angle of attack increased when flexibility was introduced – contrary to what linear static aeroelasticity predicts – inasmuch as the nonlinear model predicted a large flatwise bending that reduced the aerodynamic force component in the vertical direction.

Cesnik and Brown [3] developed a strain-based formulation for the preliminary structural design and control synthesis of high-aspect-ratio, aeroelastically-tailored flexible wings, for which anisotropic piezoelectric actuators embedded in the skin and the spar provided active wing-warping roll control. In Ref. [4], the authors refined their formulation from Ref. [4] to consider six rigid-body DOFs and fully-coupled three-dimensional bending, twisting, and extensional nonlinear deformation in the beam model.

Whereas in Refs. [3, 4] the fuselage and the tail were modeled as rigid, in Ref. [38] Cesnik and Su dealt with a fully-flexible aircraft with slender bodies. Two vehicle concepts were studied: a single-wing and a joined-wing vehicle. The latter was more susceptible to the induced flexibility of the fuselage and the tail, having the roll performance more degraded.

Shearer and Cesnik [5] coupled the 6-DOF EOMs of a reference point on a very flexible aircraft with the low-order constant strain-based nonlinear structural model of Ref. [4]. The formulation was implemented in the University of Michigan's nonlinear aeroelastic simulation toolbox (NAST or UM/NAST).

The development at the University of Michigan of a low-cost platform for nonlinear aeroelastic flight tests and future nonlinear control law studies also deserves mention: the remotely-piloted X-HALE [2]. The X-HALE aims at capturing nonlinear interactions not easily obtained or not even possible from wind tunnel tests. The aircraft is currently also being built at ITA in Brazil.

In the present paper, the methodology that assesses the validity of the assumption of small deformations is applied to the X-HALE aircraft model, in a four-meter-span, in a six-meter-span, and in an eight-meter-span configurations. Results obtained with a linear structural-dynamic, nonlinear flight-dynamic model using the described methodology are compared with the results obtained with a fully nonlinear model, comprising a geometrically-exact beam formulation [3,5,29,30], implemented in the ITA/AeroFlex program [6,33]. The aerodynamic model is the same between both models, based on Hedman's vortex-lattice method [41], whence being a quasisteady aerodynamic formulation, without unsteady effects.

With the aircraft modeled using dissimilar structural-dynamic formulations, verifications and convergence analyses become necessary to ensure that the linear and nonlinear structural-dynamic models can actually be compared with one another. The same caution is needed with respect to the aerodynamic model. With confidence that the difference between the models owes only to the difference between linear and geometrically-nonlinear approaches, conclusions can be drawn from the comparison of results. Numerical results are then presented and analyzed for different equilibrium conditions and for the flight-dynamic modes predicted by each formulation, allowing the validation of the proposed self-contained methodology to test for the validity or not of small deformations.

2 THEORETICAL BACKGROUND

In this paper, a formulation for small deformations is compared with a formulation for large deformations. The formulations are derived from first principles but independently from each other. The following subsections describe the relevant details of such formulations.

2.1 Formulation for Small Deformations

The formulation for small deformations is based on [1]. There, the equations of motion for the flexible aircraft are derived using Lagrange's equations, with the elected set of $6+n$ generalized coordinates comprising: the components of the position vector $\mathbf{R}_{O,b}$ of the origin O of a body reference frame (BRF) expressed in the body axes, b: $\mathbf{R}_{O,b} = \begin{Bmatrix} x_O & y_O & z_O \end{Bmatrix}^T$; the Euler angles providing the orientation of the BRF with respect to the inertial reference frame (IRF): ψ, θ, and ϕ; and n elastic degrees of freedom of the aircraft structure, constituting the displacement vector $\mathbf{u}_G = \begin{Bmatrix} u_1 & u_2 & \cdots & u_n \end{Bmatrix}^T$.

The aircraft is considered to be structural-dynamically represented by a finite-element model with lumped properties of inertia. The total number of mass elements is N_m. The CM of the jth mass element is at a point J, which is coincident with or rigidly connected to a structural node K.

The Earth is assumed as flat and non-rotating, and becomes an IRF [39]. The transformation matrix $\mathbf{C}_{b0}$ from the inertial frame to the body frame is obtained by a classical sequence (3-2-1) of Euler rotations, ψ, θ and ϕ [39], and is given by:

$$\mathbf{C}_{b0} = \begin{bmatrix} \cos\theta\cos\psi & \cos\theta\sin\psi & -\sin\theta \\ \cos\psi\sin\theta\sin\phi - \sin\psi\cos\phi & \sin\psi\sin\theta\sin\phi + \cos\psi\cos\phi & \cos\theta\sin\phi \\ \cos\psi\sin\theta\cos\phi + \sin\psi\sin\phi & \sin\psi\sin\theta\cos\phi - \cos\psi\sin\phi & \cos\theta\cos\phi \end{bmatrix}. \quad (1)$$

With the vector $\boldsymbol{\omega}_b = \begin{Bmatrix} p & q & r \end{Bmatrix}^T$ being the angular velocity vector of the BRF with respect to the IRF, one has [1]:

$$\widetilde{\boldsymbol{\omega}_b} = \mathbf{C}_{b0}\dot{\mathbf{C}}_{b0}^T, \tag{2}$$

with the skew-symmetric operator, $\widetilde{(\bullet)}$ or $\text{skew}\,(\bullet)$, providing an $\mathbb{R}^{3\times3}$ representation of a vector $(\bullet) \in \mathbb{R}^3$, in which, if $\mathbf{v} = \begin{Bmatrix} v_x & v_y & v_z \end{Bmatrix}^T \in \mathbb{R}^3$, then:

$$\widetilde{\mathbf{v}} = \text{skew}\,(\mathbf{v}) = \begin{bmatrix} 0 & -v_z & v_y \\ v_z & 0 & -v_x \\ -v_y & v_x & 0 \end{bmatrix}. \tag{3}$$

From Eqs. (1) and (2), one can express the angular velocity components in terms of the vector of time derivatives of the Euler angles, $\dot{\boldsymbol{\varphi}} = \begin{Bmatrix} \dot{\phi} & \dot{\theta} & \dot{\psi} \end{Bmatrix}^T$:

$$\boldsymbol{\omega}_b = \begin{bmatrix} 1 & 0 & -\sin\theta \\ 0 & \cos\phi & \sin\phi\cos\theta \\ 0 & -\sin\phi & \cos\phi\cos\theta \end{bmatrix} \dot{\boldsymbol{\varphi}} = \mathbf{H}_{\boldsymbol{\varphi}}{}^{-1}\dot{\boldsymbol{\varphi}} \tag{4}$$

With gravity assumed uniform over the airframe, the aircraft CM and center of gravity (CG) coincide, the reason why only the latter terminology will be used henceforth. Calculating and summing the contributions of each mass sub-domain to the kinetic energy, its final expression becomes [1]:

$$\begin{aligned} T &= 1/2 \sum_{j=1}^{N_m} \int_{V_j} {}^0\dot{\mathbf{R}}_I{}^T {}^0\dot{\mathbf{R}}_I \rho dV \\ &= 1/2\; m\Big({}^b\dot{\mathbf{R}}_{O,b} + \widetilde{\omega_b}\mathbf{R}_{O,b}\Big)^T \Big({}^b\dot{\mathbf{R}}_{O,b} + \widetilde{\omega_b}\mathbf{R}_{O,b}\Big) + 1/2\; \omega_b{}^T \left(\mathbf{J}_O + \Delta\mathbf{J}_O\right)\omega_b \\ &-m\Big({}^b\dot{\mathbf{R}}_{O,b} + \widetilde{\omega_b}\mathbf{R}_{O,b}\Big)^T \Big(\widetilde{\mathbf{s}_{CG,b}} + \widetilde{\mathbf{d}_{CG,b}}\Big)\omega_b + m\Big({}^b\dot{\mathbf{R}}_{O,b} + \widetilde{\omega_b}\mathbf{R}_{O,b}\Big)^T {}^b\dot{\mathbf{d}}_{CG,b} \\ &+\dot{\mathbf{u}}_G^T \mathbf{M}_{\omega G}{}^T \omega_b + 1/2\; \dot{\mathbf{u}}_G^T \mathbf{M}_{GG}\dot{\mathbf{u}}_G, \end{aligned} \tag{5}$$

with:

$$\mathbf{J}_O = \frac{1}{2}\sum_{j=1}^{N_m} \Big(m_j \widetilde{\mathbf{s}_{OJ,b}}{}^T \widetilde{\mathbf{s}_{OJ,b}} + \mathbf{J}_j\Big), \tag{6}$$

$$\Delta\mathbf{J}_O = 2\sum_{j=1}^{N_m} m_j \left(\widetilde{\mathbf{s}_{OJ,b}}^T \widetilde{\mathbf{d}_{K,b}} + \widetilde{\mathbf{s}_{OK,b}}^T \mathbf{s}_{KJ,b}\boldsymbol{\varphi}_K{}^T - \widetilde{\mathbf{s}_{OJ,b}}^T \boldsymbol{\varphi}_K \mathbf{s}_{KJ,b}{}^T\right) \tag{7}$$

$$+\sum_{j=1}^{N_m} m_j \left(\widetilde{\mathbf{d}_{K,b}}^T \widetilde{\mathbf{d}_{K,b}} + 2\left(\widetilde{\mathbf{d}_{K,b}}^T \mathbf{s}_{KJ,b}\boldsymbol{\varphi}_K{}^T - \widetilde{\mathbf{d}_{K,b}}^T \boldsymbol{\varphi}_K \mathbf{s}_{KJ,b}{}^T\right)\right)$$

$$+\sum_{j=1}^{N_m} \left(\left(m_j \widetilde{\mathbf{s}_{KJ,b}}^T \widetilde{\mathbf{s}_{KJ,b}} + \mathbf{J}_j\right)\boldsymbol{\varphi}_K \boldsymbol{\varphi}_K{}^T\right)$$

$$+\sum_{j=1}^{N_m} \left(\widetilde{\boldsymbol{\varphi}_K}\left(2\mathbf{J}_j - \mathrm{tr}\left(\mathbf{J}_j\right)\mathbf{I}_3 - \widetilde{\boldsymbol{\varphi}_K}\left(m_j \mathbf{s}_{KJ,b}\mathbf{s}_{KJ,b}{}^T - \mathbf{J}_j + 1/2\ \mathrm{tr}\left(\mathbf{J}_j\right)\mathbf{I}_3\right)\right)\right),$$

$$\mathbf{M}_{GG} = \sum_{j=1}^{N_m} m_j \left(\mathbf{U}_{t,b,KG}{}^T \mathbf{U}_{t,b,KG} - \mathbf{U}_{t,b,KG}{}^T \widetilde{\mathbf{s}_{KJ,b}} \mathbf{U}_{r,b,KG} - \mathbf{U}_{r,b,KG}{}^T \widetilde{\mathbf{s}_{KJ,b}}^T \mathbf{U}_{t,b,KG}\right) \tag{8}$$

$$+\sum_{j=1}^{N_m} \mathbf{U}_{r,b,KG}{}^T \left(m_j \widetilde{\mathbf{s}_{KJ,b}}^T \widetilde{\mathbf{s}_{KJ,b}} + \mathbf{J}_j\right)\mathbf{U}_{r,b,KG},$$

$$\mathbf{s}_{CG,b} = \frac{1}{m}\sum_{j=1}^{N_m} m_j \left(\mathbf{s}_{OK,b} + \mathbf{s}_{KJ,b}\right), \tag{9}$$

$$\mathbf{d}_{CG,b} = \frac{1}{m}\sum_{j=1}^{N_m} m_j \left(\mathbf{U}_{t,b,KG} - \widetilde{\mathbf{s}_{KJ,b}}\mathbf{U}_{r,b,KG}\right)\mathbf{u}_G = \mathbf{D}_{CG,b}\mathbf{u}_G, \tag{10}$$

$$\mathbf{M}_{\boldsymbol{\omega}G}{}^T = \sum_{j=1}^{N_m} \mathbf{U}_{r,b,KG}{}^T \left(\mathbf{J}_j - \widetilde{\mathbf{U}_{r,b,KG}\mathbf{u}_G}\left(-\mathbf{J}_j + 1/2\ \mathrm{tr}\left(\mathbf{J}_j\right)\mathbf{I}_3\right)\right) \tag{11}$$

$$-\sum_{j=1}^{N_m} m_j \left(\mathbf{U}_{t,b,KG} - \widetilde{\mathbf{s}_{KJ,b}}\mathbf{U}_{r,b,KG}\right)^T \mathrm{skew}\left(\mathbf{s}_{OJ,b} + \mathbf{U}_{t,b,KG}\mathbf{u}_G - \widetilde{\mathbf{s}_{KJ,b}}\mathbf{U}_{r,b,KG}\mathbf{u}_G\right),$$

m_j the mass of the jth lumped-mass element and $\mathbf{J}_j$ the inertia matrix of the same element about its own center of mass. Moreover, m is the aircraft total mass; $\mathbf{V}_b$ is the inertial velocity vector of the origin O of the body reference frame (BRF), with components u, v, and w in the body axes; $\mathbf{s}_{(\bullet)}$ refers to the relative position vectors in the undeformed (unstrained) condition, usually called the jig shape; and $\mathbf{d}_{(\bullet)}$ stands for the changes in the $\mathbf{s}_{(\bullet)}$ vectors due to the structural deformation. The Boolean matrices $\mathbf{U}_{t,b,KG}$ and $\mathbf{U}_{r,b,KG}$ allow the recovery of the nodal displacements and rotations for the node K from the finite-element displacement vector, $\mathbf{u}_G$ [1].

The elastic strain energy for the aircraft structure modeled with finite elements reads:

$$U_{elas} = 1/2 \left(\mathbf{T}_{FEM|BRF}\mathbf{u}_G\right)^T \mathbf{K}_{FEM} \left(\mathbf{T}_{FEM|BRF}\mathbf{u}_G\right) = 1/2 \; \mathbf{u}_G{}^T \mathbf{K}_{GG} \mathbf{u}_G, \tag{12}$$

where the FEM model nodal displacements can be calculated in generic coordinate systems other than the flight-mechanics BRF coordinate system. The three-dimensional transformation matrices from the BRF to such coordinate systems are collected in the block-diagonal transformation matrix $\mathbf{T}_{FEM|BRF}$, such that the original FEM stiffness matrix, $\mathbf{K}_{FEM}$, is transformed to $\mathbf{K}_{GG} = \mathbf{T}_{FEM|BRF}{}^T \mathbf{K}_{FEM} \mathbf{T}_{FEM|BRF}$.

The gravitational potential energy is given by:

$$\begin{aligned} U_{grav} &= -\sum_{j=1}^{N_m} \int_{V_j} \mathbf{g} \cdot \mathbf{R}_I \rho dV \\ &= -m\mathbf{g}_b{}^T \left(\mathbf{R}_{O,b} + \mathbf{s}_{CG,b} + \mathbf{d}_{CG,b}\right). \end{aligned} \tag{13}$$

At last, structural dissipation due to damping forces of viscous nature is assumed [40]:

$$\mathcal{F} = 1/2 \; \dot{\mathbf{u}}_G^T \mathbf{B}_{GG} \dot{\mathbf{u}}_G. \tag{14}$$

The generalized forces comprise the aerodynamic and the propulsive forces. The former are calculated considering the use of the vortex-lattice method (VLM) [41]. On the other hand, the propulsive forces can be modeled as concentrated thrust forces acting on the thrust center of each one of the N_E engines. Considering that a matrix $\mathbf{C}_{be}$ transforms the thrust force from an engine frame – whose x axis is aligned with the thrust line – to the body frame, one has the concentrated force $\mathbf{T}_{e,b} = \mathbf{C}_{be}\mathbf{e}_{3,1}T_e$ applied at a point E whose position vector with respect to O in the undeformed aircraft is $\mathbf{s}_{OE,b}$. The notation $\mathbf{e}_{N,i}$ a column matrix with N entries of which the ith is equal to 1 and all the others are null.

Every thrust center is also considered to be coincident with or rigidly connected to a structural node K_E in the FEM model of the aircraft, with associated Boolean matrices $\mathbf{U}_{t,b,K_EG}$ and $\mathbf{U}_{r,b,K_EG}$. The translations and the rotations of the thrust center are then given by the vectors $\mathbf{d}_{e,b} = \left(\mathbf{U}_{t,b,K_EG} - \widetilde{\mathbf{s}_{K_EE,b}}\mathbf{U}_{r,b,K_EG}\right)\mathbf{u}_G$ and $\boldsymbol{\varphi}_e = \mathbf{U}_{r,b,K_EG}\mathbf{u}_G$, respectively, with $\mathbf{s}_{K_EE,b}$ the position vector of the thrust center with respect to K_E.

Under small deformations, the thrust vector is $\mathbf{T}_{e,b} = \left(\mathbf{C}_{be} + \widetilde{\boldsymbol{\varphi}_e}\right)\mathbf{e}_{3,1}T_e$ and the thrust center is $\mathbf{s}_{OE,b} + \mathbf{d}_{e,b}$. The concentrated propulsive force can be represented as a distributed force by means of a three-dimensional Dirac's delta function [21]. As a result, the final expressions for the generalized forces in the BRF DOFs become:

$$\mathbf{Q}_{\mathbf{R}_{O,b}} = \mathbf{F}_{a,b} + \sum_{e=1}^{N_E} \mathbf{C}_{be}T_e\mathbf{e}_{3,1} + \Delta\mathbf{F}_{a,b} + \sum_{e=1}^{N_E} \widetilde{\boldsymbol{\varphi}_e}T_e\mathbf{e}_{3,1} = \mathbf{F}_b + \Delta\mathbf{F}_b, \tag{15}$$

$$\mathbf{Q}_{\boldsymbol{\varphi}} = \left(\mathbf{H}_{\boldsymbol{\varphi}}{}^{-1}\right)^T \left(\mathbf{M}_{a,O,b} + \sum_{e=1}^{N_E} \widetilde{\mathbf{s}_{OE,b}} T_e \mathbf{C}_{be} \mathbf{e}_{3,1} + \Delta\mathbf{M}_{a,O,b} + \Delta\mathbf{M}_{p,O,b} + \widetilde{\mathbf{R}_{O,b}} \mathbf{Q}_{\mathbf{R}_{O,b}} \right) \quad (16)$$
$$= \left(\mathbf{H}_{\boldsymbol{\varphi}}{}^{-1}\right)^T \left(\mathbf{M}_{O,b} + \Delta\mathbf{M}_{O,b} + \widetilde{\mathbf{R}_{O,b}} \left(\mathbf{F}_b + \Delta\mathbf{F}_b\right) \right),$$

where $\mathbf{F}_{a,b}$ and $\mathbf{M}_{a,O,b}$ are the net aerodynamic force and moment vectors, respectively, associated with the rigid airframe; $\Delta\mathbf{F}_{a,b}$ and $\Delta\mathbf{M}_{a,O,b}$ are the net incremental aerodynamic force and moment vectors, respectively, due to the elastic motion; and:

$$\Delta\mathbf{M}_{p,O,b} = \sum_{e=1}^{N_E} T_e \left(\widetilde{\mathbf{s}_{OE,b}} (\widetilde{\mathbf{U}_{r,b,K_EG}} \mathbf{u}_G) + \text{skew}\left(\left(\mathbf{U}_{t,b,K_EG} - \widetilde{\mathbf{s}_{K_EE,b}} \mathbf{U}_{r,b,K_EG} \right) \mathbf{u}_G \right) \mathbf{C}_{be} \right) \mathbf{e}_{3,1}$$

is the net linearized incremental propulsive moment vector due to the structural displacements. All the moments are about O.

The incremental aerodynamic loads are modeled with the VLM [41]. Hence, the aerodynamic forces and moments are concentrated on a discrete set of N_P aerodynamic grid points, located at the centroids of the VLM boxes, with N_P equal to the number of boxes in the discretization of the aerodynamic model. The structural displacements at the aerodynamic grid points are calculated with a linear transformation matrix $\mathbf{G}_{AG}$ that provides the vector of aerodynamic normal and rotational displacements, $\mathbf{u}_A$, from the structural displacements, $\mathbf{u}_G$: $\mathbf{u}_A = \mathbf{G}_{AG}\mathbf{u}_G$. Each aerodynamic grid point has two degrees of freedom – plunge and pitch – and the length N_A of the $\mathbf{u}_A$ vector is then $N_A = 2N_P$. The vector containing the aerodynamic forces and moments at the aerodynamic grid points is $\mathbf{P}_A$. With this rationale, the vector of generalized force in the $\mathbf{u}_G$ DOFs reads:

$$\mathbf{Q}_G = \mathbf{G}_{AG}{}^T \mathbf{P}_A + \sum_{e=1}^{N_E} \left(\mathbf{U}_{t,b,K_EG} - \widetilde{\mathbf{s}_{K_EE,b}} \mathbf{U}_{r,b,K_EG} \right)^T T_e \left(\mathbf{C}_{be} \mathbf{e}_{3,1} - \widetilde{\mathbf{e}_{3,1}} \mathbf{U}_{r,b,K_EG} \mathbf{u}_G \right) \quad (17)$$

The equations of motion for the constrained flexible aircraft are obtained by the substitution of the energy expressions, Eqs. (5), (12) and (13); Rayleigh's dissipation function, Eq. (14); and the generalized forces, Eqs. (15), (16) and (17), into Lagrange's equations [1]. It is assumed in the derivation that no change in the aircraft mass occurs with time. The equations of motions are given by:

$$\begin{gathered} m\dot{\mathbf{V}}_b + m\widetilde{\boldsymbol{\omega}_b}\mathbf{V}_b - m\widetilde{\mathbf{s}_{CG,b}}\dot{\boldsymbol{\omega}}_b - m\widetilde{\boldsymbol{\omega}_b}\widetilde{\mathbf{s}_{CG,b}}\boldsymbol{\omega}_b \\ +m\widetilde{\dot{\boldsymbol{\omega}}_b}\mathbf{D}_{CG,b}\mathbf{u}_G + 2m\widetilde{\boldsymbol{\omega}_b}\mathbf{D}_{CG,b}\dot{\mathbf{u}}_G + m\widetilde{\boldsymbol{\omega}_b}\widetilde{\boldsymbol{\omega}_b}\mathbf{D}_{CG,b}\mathbf{u}_G \\ +m\mathbf{D}_{CG,b}\ddot{\mathbf{u}}_G = m\mathbf{g}_b + \mathbf{F}_b + \Delta\mathbf{F}_b, \end{gathered} \quad (18)$$

$$
\begin{aligned}
&\mathbf{J}_O\dot{\boldsymbol{\omega}}_b + \widetilde{\boldsymbol{\omega}_b}\mathbf{J}_O\boldsymbol{\omega}_b + m\widetilde{\mathbf{s}_{CG,b}}\left(\dot{\mathbf{V}}_b + \widetilde{\boldsymbol{\omega}_b}\mathbf{V}_b\right) \\
&+m\widetilde{\mathbf{D}_{CG,b}\mathbf{u}_G}\left(\dot{\mathbf{V}}_b + \widetilde{\boldsymbol{\omega}_b}\mathbf{V}_b\right) \\
&+\Delta\mathbf{J'}_O\dot{\boldsymbol{\omega}}_b + \widetilde{\boldsymbol{\omega}_b}\Delta\mathbf{J'}_O\boldsymbol{\omega}_b + \Delta\dot{\mathbf{J}}'_O\boldsymbol{\omega}_b \\
&+\dot{\mathbf{M}}_{\boldsymbol{\omega}G}\dot{\mathbf{u}}_G + \mathbf{M}_{\boldsymbol{\omega}G}\ddot{\mathbf{u}}_G + \widetilde{\boldsymbol{\omega}_b}\mathbf{M}_{\boldsymbol{\omega}G}\dot{\mathbf{u}}_G \\
&= m\widetilde{\mathbf{s}_{CG,b}}\mathbf{g}_b + m\widetilde{\mathbf{D}_{CG,b}\mathbf{u}_G}\mathbf{g}_b + \mathbf{M}_{O,b} + \Delta\mathbf{M}_{O,b},
\end{aligned} \tag{19}
$$

$$
\begin{aligned}
&\mathbf{M}_{GG}\ddot{\mathbf{u}}_G + \mathbf{B}_{GG}\dot{\mathbf{u}}_G + \mathbf{K}_{GG}\mathbf{u}_G \\
&+m{\mathbf{D}_{CG,b}}^T\left(\dot{\mathbf{V}}_b + \widetilde{\boldsymbol{\omega}_b}\mathbf{V}_b\right) + {\mathbf{M}_{\boldsymbol{\omega}G}}^T\dot{\boldsymbol{\omega}}_b \\
&+2\dot{\mathbf{M}}^T_{\boldsymbol{\omega}G}\boldsymbol{\omega}_b - \frac{1}{2}\sum_{g=1}^{n}\mathbf{e}_{n,g}{\boldsymbol{\omega}_b}^T\frac{\partial\Delta\mathbf{J}_O}{\partial u_g}\boldsymbol{\omega}_b \\
&= m{\mathbf{D}_{CG,b}}^T\mathbf{g}_b + \mathbf{Q}_G,
\end{aligned} \tag{20}
$$

with $\Delta\mathbf{J'}_O = 1/2\ \left(\Delta\mathbf{J}_O + \Delta{\mathbf{J}_O}^T\right)$ being the symmetric inertia matrix increment, and with all the time derivatives taken in the BRF (the left superscript b was omitted for brevity).

The finite-element mass, damping and stiffness matrices are given by $\mathbf{M}_{GG}$, $\mathbf{B}_{GG}$, and $\mathbf{K}_{GG}$, respectively. The total number of elastic degrees of freedom is n.

2.1.1 Dually-Constrained Axes

The finite-element stiffness matrix, $\mathbf{K}_{GG}$, refers to an unrestrained three-dimensional structure and hence it is a positive semi-definite matrix, with a null space spanned by six linearly-independent vectors [27]. In other words, six linearly-independent rigid-body motions are allowed by the finite-element formulation in this case. This rigid-body freedom of the finite-element model is not desired, since the coordinates of the origin O and the Euler angles were already considered to be the rigid-body degrees of freedom of the BRF of the flexible aircraft. This means that six constraints are needed to eliminate the rigid-body motion from the elastic DOFs.

In the so-called dually-constrained axes [1], the origin S of the structural axes (point of no elastic displacement) is a material point (and structural node) that can be non-coincident with the origin O of the body axes. Consider that the DOFs of the node S are part of a set named the *S*-set and that the remaining DOFs are part of a set named the *D*-set. The union of the *S*- and *D*-sets recovers the *G*-set, containing all the DOFs of the FEM model. If $\mathbf{U}_{GS}$ is the Boolean matrix that locates the *S*-set DOFs in the *G*-set and $\mathbf{U}_{GD}$ is the equivalent for the *D*-set, then a rigid-body mode matrix $\boldsymbol{\Psi}_{r,S} \in \mathbb{R}^{n\times 6}$ can be obtained from [1, 43]:

$$
\boldsymbol{\Psi}_{r,S} = \begin{bmatrix}\mathbf{U}_{GD} & \mathbf{U}_{GS}\end{bmatrix}\begin{bmatrix}-\left({\mathbf{U}_{GD}}^T\mathbf{K}_{GG}\mathbf{U}_{GD}\right)^{-1}\left({\mathbf{U}_{GD}}^T\mathbf{K}_{GG}\mathbf{U}_{GS}\right) \\ \mathbf{I}_6\end{bmatrix}, \tag{21}
$$

where $\mathbf{I}_N$ denotes the identity matrix of order N. The rigid-body modes can be shown to depend exclusively on the geometry of the FEM model [27] and on the selected node S, about which the rigid-body rotations occur.

For the dually-constrained axes, the constraint is that $\mathbf{u}_S = \mathbf{0}$, corresponding to a clamped boundary condition at the node S. Due to the difficulty in attaining the same level of fidelity in the aerodynamic forces and moments acting on the rigid-body DOFs and the generalized aerodynamic forces acting on the elastic DOFs, the satisfaction of the equations of motion (2.1) and (2.1) does not ensure that Eq. (2.1) is satisfied. In other words, the finite-element model can present rigid-body accelerations, $\mathbf{\Psi}_{r,S}\ddot{\boldsymbol{\xi}}_S$, due to the uneven level of fidelity. To avoid this, a d'Alembert force vector [43], $-\mathbf{M}_{GG}\mathbf{\Psi}_{r,S}\ddot{\boldsymbol{\xi}}_S$, is included in Eq. (2.1), which is then left-multiplied by ${\mathbf{\Psi}_{r,S}}^T$, allowing the determination of $\ddot{\boldsymbol{\xi}}_S$. This procedure yields the final equations of motion in the elastic DOFs [1, 43]:

$$\begin{aligned}
&\mathbf{P}_r\mathbf{M}_{GG}\ddot{\mathbf{u}}_G + \mathbf{P}_r\mathbf{B}_{GG}\dot{\mathbf{u}}_G + \mathbf{P}_r\mathbf{K}_{GG}\mathbf{u}_G \\
&+m{\mathbf{P}_r\mathbf{D}_{CG,b}}^T\left(\dot{\mathbf{V}}_b + \widetilde{\boldsymbol{\omega}_b}\mathbf{V}_b\right) + {\mathbf{P}_r\mathbf{M}_{\boldsymbol{\omega}G}}^T\dot{\boldsymbol{\omega}}_b \\
&+2\mathbf{P}_r\dot{\mathbf{M}}^T_{\boldsymbol{\omega}G}\boldsymbol{\omega}_b - \frac{1}{2}\mathbf{P}_r\sum_{g=1}^{n}{\mathbf{e}_{n,g}\boldsymbol{\omega}_b}^T\frac{\partial\Delta\mathbf{J}_O}{\partial u_g}\boldsymbol{\omega}_b \\
&= m{\mathbf{P}_r\mathbf{D}_{CG,b}}^T\mathbf{g}_b + \mathbf{P}_r\mathbf{Q}_G,
\end{aligned} \tag{22}$$

with $\mathbf{P}_r = \mathbf{I}_n - \mathbf{M}_{GG}\mathbf{\Psi}_{r,S}{\mathbf{M}_{rr,S}}^{-1}{\mathbf{\Psi}_{r,S}}^T$ the so-called inertia-relief projection matrix [43] and $\mathbf{M}_{rr,S} = {\mathbf{\Psi}_{r,S}}^T\mathbf{M}_{GG}\mathbf{\Psi}_{r,S}$ the FEM rigid-body mass matrix.

With the inertia relief effect taken into account, any structural node can have its displacements assumed null in Eq. (22), e.g., $\mathbf{u}_S = \mathbf{0}$, which implies $\mathbf{u}_G = \mathbf{U}_{GD}\mathbf{u}_D$. Hence, in the case of the dually-constrained axes, the origin O keeps its position constant with respect to the undeformed aircraft (first constraint) and the structural node S is the point where the undeformed and the deformed airframes coincide at any time instant (second constraint).

2.1.2 Aerodynamic Model

The aerodynamic loads acting on the flexible aircraft can be calculated as the superposition of loads that would be obtained were the airframe perfectly rigid with incremental loads due to the structural deformation. In this case, the aerodynamic data for the rigid aircraft consists of tables of non-dimensional force and moment coefficients and do not comprise any structural flexibility effect. To obtain the generalized aerodynamic loads related to the structural motion, the VLM [41] is used in this paper, yielding the following linear system of equations:

$$\mathbf{A}^{-1}\Delta\mathbf{C}_\mathbf{p} = \mathbf{w}, \tag{23}$$

where $\mathbf{w} \in \mathbb{R}^{N_P}$ is the vector of non-dimensional normalwashes at the N_P panel (box) control points; $\Delta\mathbf{C}_\mathbf{p} \in \mathbb{R}^{N_P}$ is the vector of panel pressure coefficient differences; and $\mathbf{A} \in \mathbb{R}^{N_P \times N_P}$ is

the AIC (aerodynamic influence coefficient) matrix. The VLM AIC matrix is dependent upon the geometry and discretization of the aerodynamic lifting surfaces in the model. Dependence on the Mach number, M, is neglected in this paper, since compressibility effects are not present in the cases studied here.

The body frame of reference used to calculate the aerodynamic loads is defined as an aerodynamic reference frame (ARF). Its inertial angular rates are written in the ARF coordinate system as p_a, q_a, and r_a, and its inertial velocity has the components u_a, v_a, and w_a in the same system [1]. The rigid-body motion of the aircraft then contributes to the generalized aerodynamic forces (GAFs) in the elastic DOFs in terms of p_a, q_a, r_a, u_a, v_a, w_a, the control surface deflections and other possible rigid-body variables. The elastic deformation of the structure measured with respect to the ARF, given by the vector $\mathbf{u}_{G/A}$, contributes to the incremental GAFs. The total GAFs are then given by [1]:

$$\mathbf{Q}_G = \bar{q}\mathbf{G}_{AG}{}^T\mathbf{S}_{AP}\left(\Delta\mathbf{C}_{\mathbf{p},\mathbf{u}} + \Delta\mathbf{C}_{\mathbf{p},\mathbf{e}}\right). \tag{24}$$

In Eq. (24), $\bar{q}$ is the dynamic pressure; $\mathbf{G}_{AG} \in \mathbb{R}^{N_A \times n}$ is the matrix that interpolates the elastic displacements from the structural nodes to the aerodynamic grid points (at the centroids of the VLM boxes); $\mathbf{S}_{AP} \in \mathbb{R}^{N_A \times N_P}$ transforms the panel pressure coefficient differences to forces and moments at the aerodynamic grid points, and is usually called an integration matrix; $\Delta\mathbf{C}_{\mathbf{p},\mathbf{u}}$ is the vector of panel pressure coefficient differences related to the rigid-body states, without elastic deformation; and $\Delta\mathbf{C}_{\mathbf{p},\mathbf{e}}$ is the vector of panel incremental pressure coefficient differences.

The elastic contribution to the generalized aerodynamic forces is calculated with the equation [1]:

$$\Delta\mathbf{C}_{\mathbf{p},\mathbf{e}} = \mathbf{A}\left(\mathbf{D}_{PA,0}\mathbf{G}_{AG}\mathbf{u}_{G/A} + \frac{b_w}{V_a}\mathbf{D}_{PA,1}\mathbf{G}_{AG}\dot{\mathbf{u}}_{G/A}\right), \tag{25}$$

where $\mathbf{D}_{PA,0}, \mathbf{D}_{PA,1} \in \mathbb{R}^{N_P \times N_A}$ are the differentiation matrices that allow the calculation of control point normalwashes at three quarters of the boxes' mean chords from the displacements at the aerodynamic grid points, respectively; b_w is the reference wing semi-chord; and $N_A = 2N_P$ is the total number of aerodynamic degrees of freedom (each panel has two DOFs, plunge and pitch).

The integration and differentiation matrices in Eq. (25) are given by:

$$\mathbf{S}_{AP} = \sum_{k=1}^{N_P} S_k\left(\mathbf{e}_{N_A,2k-1}\mathbf{e}_{N_P,k}{}^T + \mathbf{e}_{N_A,2k}\mathbf{e}_{N_P,k}{}^T\left(x_{050,k} - x_{025,k}\right)\right), \tag{26}$$

$$\mathbf{D}_{PA,0} = \sum_{k=1}^{N_P} \mathbf{e}_{N_P,k}\mathbf{e}_{N_A,2k}{}^T, \tag{27}$$

$$\mathbf{D}_{PA,1} = \frac{1}{b_w}\sum_{k=1}^{N_P}\left(\mathbf{e}_{N_P,k}\mathbf{e}_{N_A,2k-1}{}^T + \mathbf{e}_{N_P,k}\mathbf{e}_{N_A,2k}{}^T\left(x_{075,k} - x_{025,k}\right)\right), \tag{28}$$

with $x_{025,k}, x_{050,k}, x_{075,k}$ the x coordinates, in the aerodynamic model coordinate system, of the points at one quarter, one half and three quarters of the kth aerodynamic box (panel) mean chord; and S_k the kth aerodynamic box area.

In this paper, the aerodynamic reference frame is modeled with attached axes [1]. This means that the origin A is coincident with or rigidly connected to a material point C that remains fixed when structural deformation occurs. For small elastic deformations, one can write:

$$\mathbf{u}_{G/A} = \mathbf{u}_G - \mathbf{\Psi}_{r,A}\mathbf{u}_{A,b}, \tag{29}$$

$$\mathbf{u}_{A,b} = \begin{bmatrix} \mathbf{I}_3 & -\widetilde{\mathbf{s}_{CA,b}} \\ \mathbf{0}_3 & \mathbf{I}_3 \end{bmatrix} \mathbf{U}_c{}^T \mathbf{u}_G, \tag{30}$$

where $\mathbf{\Psi}_{r,A}$ is the rigid-body mode matrix of the free-free aircraft calculated with origin at A [1] and $\mathbf{U}_C$ is the Boolean matrix that selects the node C degrees of freedom among all DOFs. The left multiplication of Eq. (29) by $\mathbf{K}_{GG}$ and the partition of $\mathbf{u}_{G/A}$ into its fixed DOFs, $\mathbf{u}_{G/A,c} = \mathbf{0}_{6\times 1}$, and free DOFs, $\mathbf{u}_{G/A,f}$, i.e., $\mathbf{u}_{G/A} = \mathbf{U}_f\mathbf{u}_{G/A,f} + \mathbf{U}_c\mathbf{u}_{G/A,c} = \mathbf{U}_f\mathbf{u}_{G/A,f}$, allow one to determine that [1]:

$$\mathbf{u}_{G/A} = \mathbf{U}_f\left(\mathbf{U}_f{}^T\mathbf{K}_{GG}\mathbf{U}_f\right)^{-1}\mathbf{U}_f{}^T\mathbf{K}_{GG}\mathbf{u}_G. \tag{31}$$

The position vector of A in the BRF reads:

$$\mathbf{R}_{A,b} = \mathbf{R}_{O,b} + \mathbf{s}_{OA,b} + \begin{bmatrix} \mathbf{I}_3 & \mathbf{0}_3 \end{bmatrix} \mathbf{u}_{A,b}. \tag{32}$$

A matrix $\mathbf{C}_{ab}$ generated with the small rotations $\boldsymbol{\varphi}_A = \begin{bmatrix} \mathbf{0}_3 & \mathbf{I}_3 \end{bmatrix} \mathbf{u}_{A,b}$:

$$\mathbf{C}_{ab} = \mathbf{I}_3 - \widetilde{\boldsymbol{\varphi}_A} \tag{33}$$

transforms vectors from the BRF to the ARF, such that $\mathbf{R}_A$ is written in the ARF as:

$$\mathbf{R}_{A,a} = \mathbf{C}_{ab}\left(\mathbf{R}_{O,b} + \mathbf{s}_{OA,b} + \begin{bmatrix} \mathbf{I}_3 & \mathbf{0}_3 \end{bmatrix} \mathbf{u}_{A,b}\right). \tag{34}$$

The inertial velocity of A then becomes:

$$\mathbf{V}_a = {}^0\dot{\mathbf{R}}_{A,a} = \mathbf{C}_{ab}\left(\mathbf{V}_b + \begin{bmatrix} \mathbf{I}_3 & \mathbf{0}_3 \end{bmatrix} \dot{\mathbf{u}}_{A,b} + \widetilde{\boldsymbol{\omega}_b}\left(\mathbf{s}_{OA,b} + \begin{bmatrix} \mathbf{I}_3 & \mathbf{0}_3 \end{bmatrix} \mathbf{u}_{A,b}\right)\right), \tag{35}$$

from which one obtains the effective aerodynamic velocity components:

$$u_a = {\mathbf{e}_{3,1}}^{T0}\dot{\mathbf{R}}_{A,a}, \tag{36}$$
$$v_a = {\mathbf{e}_{3,2}}^{T0}\dot{\mathbf{R}}_{A,a}, \tag{37}$$
$$w_a = {\mathbf{e}_{3,3}}^{T0}\dot{\mathbf{R}}_{A,a}. \tag{38}$$

Knowing u_a, v_a, and w_a, one can calculate the corresponding V_a, α_a and β_a using the well-known relations, as in Ref. [39]. The inertial angular velocity of the ARF can be calculated as [1]:

$$\boldsymbol{\omega}_a = \mathbf{C}_{ab}\,\boldsymbol{\omega}_b + \dot{\boldsymbol{\varphi}}_A, \tag{39}$$

from which the corresponding angular rates can be obtained:

$$p_a = {\mathbf{e}_{3,1}}^{T}\boldsymbol{\omega}_a, \tag{40}$$
$$q_a = {\mathbf{e}_{3,2}}^{T}\boldsymbol{\omega}_a, \tag{41}$$
$$r_a = {\mathbf{e}_{3,3}}^{T}\boldsymbol{\omega}_a. \tag{42}$$

The aerodynamic forces and moments due to the rigid-body motion of the ARF are then given by the equations:

$$\begin{aligned}\mathbf{F}_{a,b} &= \bar{q}S_{ref}\mathbf{C}_{ba}\mathbf{C}_{av}\begin{Bmatrix}-C_D & -C_Y & -C_L\end{Bmatrix}^T,\\ \mathbf{M}_{a,O,b} &= \bar{q}S_{ref}\mathbf{C}_{ba}\begin{Bmatrix}s_wC_l & c_wC_m & s_wC_n\end{Bmatrix}^T + \widetilde{\mathbf{s}_{OA,b}}\mathbf{F}_{a,b},\end{aligned} \tag{43}$$

with $C_i = C_i\left(\alpha_a, \dot{\alpha}_a, \beta_a, \dot{\beta}_a, M, \mathrm{Re}, \omega_a, \delta_c, \ldots\right)$, $i = D, L, Y, l, m, n$ the aerodynamic force or moment coefficients for the rigid aircraft; S_{ref} the reference wing planform area; s_w the reference wing span; c_w the wing mean aerodynamic chord; and $\mathbf{C}_{av}$ given by:

$$\mathbf{C}_{av} = \begin{bmatrix}\cos\alpha_a\cos\beta_a & -\cos\alpha_a\sin\beta_a & -\sin\alpha_a\\ \sin\beta_a & \cos\beta_a & 0\\ \sin\alpha_a\cos\beta_a & -\sin\alpha_a\sin\beta_a & \cos\alpha_a\end{bmatrix} \tag{44}$$

The incremental forces and moments in the rigid-body DOFs are given by:

$$\Delta\mathbf{F}_{a,b} = \bar{q}\mathbf{C}_{ba}\mathbf{C}_{av}\sum_{k=1}^{N_P} S_k \begin{Bmatrix} -\mathbf{e}_{N_P,k}{}^T\Delta\mathbf{c}_{\mathbf{d},\mathbf{e}} \\ \mathbf{e}_{3,2}{}^T\mathbf{n}_{k,u,b}\left(\mathbf{e}_{N_P,k}{}^T\Delta\mathbf{C}_{\mathbf{p},\mathbf{e}}\right) \\ \mathbf{e}_{3,3}{}^T\mathbf{n}_{k,u,b}\left(\mathbf{e}_{N_P,k}{}^T\Delta\mathbf{C}_{\mathbf{p},\mathbf{e}}\right) \end{Bmatrix}, \tag{45}$$

$$\Delta\mathbf{M}_{a,O,b} = \Delta\mathbf{M}_{0,1} + \Delta\mathbf{M}_{1,0} + \Delta\mathbf{M}_{1,1} + \Delta\mathbf{M}_{A\to O}, \tag{46}$$

$$\Delta\mathbf{M}_{0,1} = \bar{q}\sum_{k=1}^{N_P} S_k\mathbf{C}_{ba}\left(-\text{skew}\left(\mathbf{C}_{av}\begin{Bmatrix} -\mathbf{e}_{N_P,k}{}^T\mathbf{c}_{\mathbf{d},\mathbf{u}} \\ \mathbf{e}_{3,2}{}^T\mathbf{n}_{k,u,b}\mathbf{e}_{N_P,k}{}^T\Delta\mathbf{C}_{\mathbf{p},\mathbf{u}} \\ \mathbf{e}_{3,3}{}^T\mathbf{n}_{k,u,b}\mathbf{e}_{N_P,k}{}^T\Delta\mathbf{C}_{\mathbf{p},\mathbf{u}} \end{Bmatrix}\right)\right.$$
$$\left.\mathbf{n}_{k,u,b}\left(\mathbf{e}_{N_P,k}{}^T\mathbf{C}_{025A}\mathbf{G}_{AG}\mathbf{u}_{G/A}\right)\right), \tag{47}$$

$$\Delta\mathbf{M}_{1,0} + \Delta\mathbf{M}_{1,1} = \bar{q}\sum_{k=1}^{N_P} S_k\mathbf{C}_{ba}\left(-\text{skew}\left(\mathbf{C}_{av}\begin{Bmatrix} -\mathbf{e}_{N_P,k}{}^T\Delta\mathbf{c}_{\mathbf{d},\mathbf{e}} \\ \mathbf{e}_{3,2}{}^T\mathbf{n}_{k,u,b}\left(\mathbf{e}_{N_P,k}{}^T\Delta\mathbf{C}_{\mathbf{p},\mathbf{e}}\right) \\ \mathbf{e}_{3,3}{}^T\mathbf{n}_{k,u,b}\left(\mathbf{e}_{N_P,k}{}^T\Delta\mathbf{C}_{\mathbf{p},\mathbf{e}}\right) \end{Bmatrix}\right)\right.$$
$$\left.\left(\mathbf{R}_{025,a}\mathbf{e}_{N_P,k} + \mathbf{n}_{k,u,b}\left(\mathbf{e}_{N_P,k}{}^T\mathbf{C}_{025A}\mathbf{G}_{AG}\mathbf{u}_{G/A}\right)\right)\right), \tag{48}$$

$$\Delta\mathbf{M}_{A\to O} = \text{skew}\left(\begin{bmatrix}\mathbf{I}_3 & \mathbf{0}_3\end{bmatrix}\mathbf{u}_{A,b}\right)\mathbf{F}_{a,b} + \text{skew}\left(\mathbf{s}_{OA,b} + \begin{bmatrix}\mathbf{I}_3 & \mathbf{0}_3\end{bmatrix}\mathbf{u}_{A,b}\right)\Delta\mathbf{F}_{a,b}, \tag{49}$$

where $\Delta\mathbf{c}_{\mathbf{d},\mathbf{e}} = \Delta\mathbf{c}_{\mathbf{d},\mathbf{ind},\mathbf{e}}$ is the vector of panel drag coefficient disturbances due to the structural deformation, with $\Delta\mathbf{c}_{\mathbf{d},\mathbf{ind},\mathbf{e}}$ the vector of panel induced drag disturbances; $\mathbf{n}_{k,u,b}$ is the normal vector to each panel in its undeformed position, with components written in the BRF coordinate system; $\Delta\mathbf{C}_{\mathbf{p},\mathbf{e}} = \mathbf{A}'\mathbf{w}_{\mathbf{elas}}$; $\mathbf{C}_{025A} \in \mathbb{R}^{N_P\times N_A}$ is a matrix that transforms the aerodynamic grid points' displacements to the normal displacement of the points at 25% of the mean chord of the panels; $\mathbf{R}_{025,a} \in \mathbb{R}^{3\times N_P}$ is a matrix containing the three-dimensional coordinates, in the ARF coordinate system, of the points at 25% of the mean chord of all the panels; $\mathbf{c}_{\mathbf{d},\mathbf{u}} = \mathbf{c}_{\mathbf{d},\mathbf{0}} + \mathbf{c}_{\mathbf{d},\mathbf{ind},\mathbf{u}}$ is the vector of panel drag coefficients due to the rigid-body states: $\mathbf{c}_{\mathbf{d},\mathbf{0}}$ is the vector of panel zero-lift drag coefficients, approximated as $\mathbf{c}_{\mathbf{d},\mathbf{0}} = \sum_{k=1}^{N_P}\mathbf{e}_{N_P,k}\left(S_{ref}/\sum_{k=1}^{N_P} S_k\right)C_{D,0}$; and $\mathbf{c}_{\mathbf{d},\mathbf{ind},\mathbf{u}}$ is the vector of panel induced drag coefficients due to $\Delta\mathbf{C}_{\mathbf{p},\mathbf{u}}$.

The rigid-body and the incremental induced drags are calculated based on the methodology of Ref. [51].

2.1.3 Shape functions and stiffness matrix of elastic elements for small deformations

In the present paper, it is assumed that the aircraft structure is modeled with beam elements. The adopted beam element in three dimensions has two nodes and twelve degrees of freedom. The element shape functions are given by:

$$u_e\left(x_e, y_e, z_e\right) = a_0 + a_1x_e - \frac{\partial w_e}{\partial x_e}x_e - \frac{\partial v_e}{\partial x_e}x_e, \tag{50}$$

$$v_e\left(x_e, y_e, z_e\right) = b_0 + b_1x_e + b_2x_e^2 + b_3x_e^3 - \Theta_e\left(x_e, y_e, z_e\right)z_e, \tag{51}$$

$$w_e\left(x_e, y_e, z_e\right) = c_0 + c_1x_e + c_2x_e^2 + c_3x_e^3 + \Theta_e\left(x_e, y_e, z_e\right)y_e, \tag{52}$$

where $u_e\left(x_e, y_e, z_e\right)$ is the axial displacement shape function and $v_e\left(x_e, y_e, z_e\right)$ and $w_e\left(x_e, y_e, z_e\right)$ are the edgewise and flatwise displacements' shape functions, respectively. The set of shape functions becomes complete with the twist angle shape function:

$$\Theta_e\left(x_e, y_e, z_e\right) = d_0 + d_1 x_e. \tag{53}$$

yielding, at last:

$$\begin{aligned} u_e\left(x_e, y_e, z_e\right) &= a_0 + a_1 x_e - \left(c_1 + 2c_2 x_e + 3c_3 x_e^2 - d_1 z_e\right) x_e \\ &\quad - \left(b_1 + 2b_2 x_e + 3b_3 x_e^2 + d_1 y_e\right) x_e, \end{aligned} \tag{54}$$

$$v_e\left(x_e, y_e, z_e\right) = b_0 + b_1 x_e + b_2 x_e^2 + b_3 x_e^3 - d_0 z_e - d_1 x_e z_e, \tag{55}$$

$$w_e\left(x_e, y_e, z_e\right) = c_0 + c_1 x_e + c_2 x_e^2 + c_3 x_e^3 + d_0 y_e + d_1 x_e y_e. \tag{56}$$

The twelve degrees of freedom of the beam finite element are whence considered to be given by: $u_{e1} = u_e\left(0,0,0\right)$, $v_{e1} = v_e\left(0,0,0\right)$, $w_{e1} = w_e\left(0,0,0\right)$, $\phi_{e1} = \Theta_e\left(0,0,0\right)$, $\theta_{e1} = -\frac{\partial w_e}{\partial x_e}\left(0,0,0\right)$, $\psi_{e1} = \frac{\partial v_e}{\partial x_e}\left(0,0,0\right)$, $u_{e2} = u_e\left(L_e,0,0\right)$, $v_{e2} = v_e\left(L_e,0,0\right)$, $w_{e2} = w_e\left(L_e,0,0\right)$, $\phi_{e2} = \Theta_e\left(L_e,0,0\right)$, $\theta_{e2} = -\frac{\partial w_e}{\partial x_e}\left(L_e,0,0\right)$, and $\psi_{e2} = \frac{\partial v_e}{\partial x_e}\left(L_e,0,0\right)$, where L_e is the element length.

The element elastic strains are given by:

$$\epsilon_x = \frac{\partial u_e}{x_e}, \tag{57}$$

$$\epsilon_y = -\nu\epsilon_x, \tag{58}$$

$$\epsilon_z = -\nu\epsilon_x, \tag{59}$$

$$\gamma_{xy} = \frac{\partial v_e}{x_e} + \frac{\partial u_e}{y_e}, \tag{60}$$

$$\gamma_{xz} = \frac{\partial w_e}{x_e} + \frac{\partial u_e}{z_e}, \tag{61}$$

$$\gamma_{yz} = \frac{\partial w_e}{y_e} + \frac{\partial v_e}{z_e}, \tag{62}$$

where ν is Poisson's ratio for the beam material and Eqs. (54-56) shall be considered. Using Voigt's notation, the element strains may be collected in a six-dimensional column matrix, $\boldsymbol{\epsilon} = \left\{\epsilon_x \quad \epsilon_y \quad \epsilon_z \quad \gamma_{xy} \quad \gamma_{xz} \quad \gamma_{yz}\right\}^T$, which is itself a linear function of the element twelve degrees of freedom. The element stresses can be calculated with the consideration of the isotropic linear elastic material stiffness matrix, $\mathbf{C}$:

$$\mathbf{C} = \begin{bmatrix} \lambda+2\mu & \lambda & \lambda & 0 & 0 & 0 \\ \lambda & \lambda+2\mu & \lambda & 0 & 0 & 0 \\ \lambda & \lambda & \lambda+2\mu & 0 & 0 & 0 \\ 0 & 0 & 0 & \mu & 0 & 0 \\ 0 & 0 & 0 & 0 & \mu & 0 \\ 0 & 0 & 0 & 0 & 0 & \mu \end{bmatrix}, \tag{63}$$

so that:

$$\boldsymbol{\sigma} = \mathbf{C}\boldsymbol{\epsilon}. \tag{64}$$

In Eq. (63), $\lambda = \frac{E\nu}{(1+\nu)(1-2\nu)}$ and $\mu = G = \frac{E}{2(1+\nu)}$, where E and G are the material Young's and shear moduli, respectively. The element stiffness matrix $\mathbf{K}_{ee}$ is such that the element strain energy satisfies:

$$U_e = \frac{1}{2}\iiint_{element} \boldsymbol{\sigma}^T \boldsymbol{\epsilon} dV = \frac{1}{2}\mathbf{u}_e{}^T \mathbf{K}_{ee} \mathbf{u}_e, \tag{65}$$

with $\mathbf{u}_e = \begin{Bmatrix} u_{e1} & v_{e1} & w_{e1} & \phi_{e1} & \theta_{e1} & \psi_{e1} & u_{e2} & v_{e2} & w_{e2} & \phi_{e2} & \theta_{e2} & \psi_{e2} \end{Bmatrix}^T$. It can be demonstrated that:

$$\mathbf{K}_{ee} = \tag{66}$$

$$E \begin{bmatrix}
\frac{A}{L_e} & 0 & 0 & 0 & \frac{Az}{L_e} & -\frac{Ay}{L_e} & -\frac{A}{L_e} & 0 & 0 & 0 & -\frac{Az}{L_e} & \frac{Ay}{L_e} \\
 & \frac{12I_z}{{L_e}^3} & \frac{12I_{yz}}{{L_e}^3} & 0 & -\frac{6I_{yz}}{{L_e}^2} & \frac{6I_z}{{L_e}^2} & 0 & -\frac{12I_z}{{L_e}^3} & -\frac{12I_{yz}}{{L_e}^3} & 0 & -\frac{6I_{yz}}{{L_e}^2} & \frac{6I_z}{{L_e}^2} \\
 & & \frac{12I_y}{{L_e}^3} & 0 & -\frac{6I_y}{{L_e}^2} & \frac{6I_{yz}}{{L_e}^2} & 0 & -\frac{12I_{yz}}{{L_e}^3} & -\frac{12I_y}{{L_e}^3} & 0 & -\frac{6I_y}{{L_e}^2} & \frac{6I_{yz}}{{L_e}^2} \\
 & & & \frac{GJ}{EL_e} & 0 & 0 & 0 & 0 & 0 & -\frac{GJ}{EL_e} & 0 & 0 \\
 & & & & \frac{4I_y}{L_e} & -\frac{4I_{yz}}{L_e} & -\frac{Az}{L_e} & \frac{6I_{yz}}{{L_e}^2} & \frac{6I_y}{{L_e}^2} & 0 & \frac{2I_y}{L_e} & -\frac{2I_{yz}}{L_e} \\
 & & & & & \frac{4I_z}{L_e} & \frac{Ay}{L_e} & -\frac{6I_z}{{L_e}^2} & -\frac{6I_{yz}}{{L_e}^2} & 0 & -\frac{2I_{yz}}{L_e} & \frac{2I_z}{L_e} \\
 & & & & & & \frac{A}{L_e} & 0 & 0 & 0 & \frac{Az}{L_e} & -\frac{Ay}{L_e} \\
 & & & & & & & \frac{12I_z}{{L_e}^3} & \frac{12I_{yz}}{{L_e}^3} & 0 & \frac{6I_{yz}}{{L_e}^2} & -\frac{6I_z}{{L_e}^2} \\
 & & & & & & & & \frac{12I_y}{{L_e}^3} & 0 & \frac{6I_y}{{L_e}^2} & -\frac{6I_{yz}}{{L_e}^2} \\
 & & & & & & & & & \frac{GJ}{EL_e} & 0 & 0 \\
 & & & & & & & & & & \frac{4I_y}{L_e} & -\frac{4I_{yz}}{L_e} \\
 & & & & & & & & & & & \frac{4I_z}{L_e}
\end{bmatrix}, \tag{66}$$

where A is the cross-sectional area, I_y and I_z are the cross-sectional area moments of inertia, J is the torsion constant, I_{yz} is the cross-sectional area product of inertia, and y and z are coordinates accounting for the possible eccentricity between the beam axis and the shear center.

Although a consistent mass matrix can also be obtained for the beam element based on the material density and the element shape functions, the flight-dynamic formulation is not prepared to deal with consistent masses, due to resulting inertial coupling between the two beam element nodes. Rather, a lumped mass matrix is generated by transferring to each node half of the mass of the element, as well as the first and second moments of inertia and the products of inertia due to each half of the element.

2.2 Strain-based geometrically-nonlinear beam formulation

The main goal of this section is to provide a brief review of the strain-based geometrically-nonlinear beam model. The reader is referred, for instance, to Refs. [29], [30], [31], and

[32] for a complete description and derivation of these equations. We developed a toolbox (ITA/AeroFlex) that implements this formulation [33].

The key idea here is to use the following kinematic relationship, which relates the displacements $h(s,t)$ at a point along the beam to the strains $\epsilon(s,t)$:

$$\frac{\partial h}{\partial s}(s,t) = \mathcal{K}(s,t)h(s,t)\,, \tag{67}$$

where:

$$\mathcal{K}(s) = \begin{bmatrix} 0 & 1+\epsilon_x(s,t) & 0 & 0 \\ 0 & 0 & \kappa_z(s,t) & -\kappa_y(s,t) \\ 0 & -\kappa_z(s,t) & 0 & \kappa_x(s,t) \\ 0 & -\kappa_y(s,t) & -\kappa_x(s,t) & 0 \end{bmatrix}, \tag{68}$$

where $\epsilon_x(s,t)$ is the extensional strain, and $\kappa_x(s,t)$, $\kappa_y(s,t)$ and $\kappa_z(s,t)$ are the curvatures at point s and time t.

The flexible structure is split into elements and the strains are assumed to be constant along each element (but time-dependent), so that Eq. 67 has an analytical solution:

$$h(s,t) = e^{\mathcal{K}(s-s_0)}h_0(t)\,, \tag{69}$$

where $h_0(t)$ is the displacement of a fixed node at $x = s_0$. The matrix exponential $e^{\mathcal{K}(s-s_0)}$ exhibts a closed-form expression as presented in Ref [30].

In the ITA/AeroFlex computer program, as in previous work, flexible elements with three nodes were implemented. Furthermore, we introduced rigid elements, with time-independent null strain. These rigid elements are used to model rigid components and do not introduce new states to the model.

Using Eq. 69, it is possible to compute the displacement vector for each structural node as a function of the strains:

$$h(t) = h\left(\epsilon(t)\right)\,. \tag{70}$$

The time-derivative of the displacement vector taking into account only the motion of the structure is obtained as:

$$\dot{h}(t) = \underbrace{\frac{\partial h}{\partial \epsilon}}_{J_{h\epsilon}}\dot{\epsilon}(t)\,, \tag{71}$$

where $J_{h\epsilon}(\epsilon(t))$ is a Jacobian that relates the element strains to nodal displacements.

The rigid body motion can also be introduced by using the term $J_{hb}\beta$, where J_{hb} relates the rigid body motions to nodal displacements. Thus, the time-derivative due to both the strain rates $\dot{\epsilon}$ and the rigid body motion β (linear and angular velocity components) is given by:

$$\dot{h}(t) = J_{h\epsilon}\dot{\epsilon}(t) + J_{hb}\beta(t)\,. \tag{72}$$

The kinetic energy is computed as:

$$T = \frac{1}{2}\dot{h}^T M \dot{h}\,, \tag{73}$$

where M is the structure mass matrix, computed assuming a linear variation of the nodal speeds between the nodes. The kinetic energy can be rewritten as a function of the strain rates and rigid body velocities using Eq. 72:

$$T = \frac{1}{2}\begin{bmatrix}\dot{\epsilon} & \beta\end{bmatrix}\begin{bmatrix}M_{FF} & M_{FB}\\ M_{BF} & M_{BB}\end{bmatrix}\begin{bmatrix}\dot{\epsilon}\\ \beta\end{bmatrix}\,, \tag{74}$$

where:

$$\begin{aligned} M_{FF} &= J_{h\epsilon}^T M J_{h\epsilon}\,, \quad & M_{FB} &= J_{h\epsilon}^T M J_{hb}\,,\\ M_{BF} &= J_{hb}^T M J_{h\epsilon}\,, \quad & M_{BB} &= J_{hb}^T M J_{hb}\,. \end{aligned} \tag{75}$$

The potential (elastic) energy is given by:

$$U = \frac{1}{2}\dot{\epsilon}^T K \dot{\epsilon}\,, \tag{76}$$

where K is a block-diagonal matrix, composed of the stiffness matrices of each element K^e:

$$K^e = \begin{bmatrix} k_{11} & k_{12} & k_{13} & k_{14}\\ k_{21} & k_{22} & k_{23} & k_{24}\\ k_{31} & k_{32} & k_{33} & k_{34}\\ k_{41} & k_{42} & k_{43} & k_{44}\end{bmatrix}\,. \tag{77}$$

The off-diagonal terms allow coupling between the strains (for instance, k_{12} represents the coupling between extension and torsion).

From the Euler-Lagrange equations, the equations of motion are computed as:

$$\begin{bmatrix}M_{FF} & M_{FB}\\ M_{BF} & M_{BB}\end{bmatrix}\begin{bmatrix}\ddot{\epsilon}\\ \dot{\beta}\end{bmatrix} + \begin{bmatrix}C_{FF} & C_{FB}\\ C_{BF} & C_{BB}\end{bmatrix}\begin{bmatrix}\dot{\epsilon}\\ \beta\end{bmatrix} + \begin{bmatrix}K & 0\\ 0 & 0\end{bmatrix}\begin{bmatrix}\epsilon\\ b\end{bmatrix} = \begin{bmatrix}R_F\\ R_B\end{bmatrix} \tag{78}$$

The matrices C_{FF}, C_{BF}, C_{FB} and C_{BB} include the gyroscopic terms (due to the rotation of the rigid body and structural elements) and the structural damping term. In this work, we assume that the structural damping is proportional to the stiffness matrix: $C = \alpha K$.

R_F and R_B are the generalized forces that are applied to the airplane. They are obtained from the aerodynamic, gravitational and propulsive forces applied to each node of the structure:

$$\begin{bmatrix} R_F \\ R_B \end{bmatrix} = \begin{bmatrix} J_{p\epsilon}^T \\ J_{pb}^T \end{bmatrix} F^{pt} + \begin{bmatrix} J_{\theta\epsilon}^T \\ J_{\theta b}^T \end{bmatrix} M^{pt} + \begin{bmatrix} J_{p\epsilon}^T \\ J_{pb}^T \end{bmatrix} B^F F^{dist} + \begin{bmatrix} J_{\theta\epsilon}^T \\ J_{\theta b}^T \end{bmatrix} B^F M^{dist} + \begin{bmatrix} J_{p\epsilon}^T \\ J_{pb}^T \end{bmatrix} N\vec{g} \tag{79}$$

The Jacobian matrices $J_{p\epsilon}$ and $J_{\theta\epsilon}$ represent the relationship between structural deformations (ϵ) and nodal displacements and rotations. J_{pb} and $J_{\theta b}$ represent the relationship between rigid body degrees of freedom and nodal displacements and rotations. The Jacobian matrices are nonlinear functions of the displacement vector ϵ. Closed-form expressions for these Jacobians are presented in [30].

2.3 Correspondence between the element stiffness matrices for small and large deformations

It is fundamental for the purpose of the present paper that the same physical properties can be used indistinctly in the formulation for small deformations and in the geometrically-nonlinear formulation. The correct correspondence between the element stiffness matrices in Eq. (66) and in Eq. (77), if equal element directions and cross-section orientations are used in both elements, is given by the following equations:

$$k_{11} = EA, \tag{80}$$
$$k_{13} = EAz, \tag{81}$$
$$k_{14} = -EAy, \tag{82}$$
$$k_{22} = GJ, \tag{83}$$
$$k_{33} = EI_y, \tag{84}$$
$$k_{34} = -EI_{yz}, \tag{85}$$
$$k_{44} = EI_z. \tag{86}$$

The remaining stiffness terms in Eq. (77) that couple beam torsion with the other strains are not predicted in the formulation for small deformations, but are also less commonly employed in structural-dynamic models.

3 NUMERICAL MODELS

The X-HALE aircraft in its four-meter-span ("4m"), six-meter-span ("6m") and eight-meter-span ("8m") configurations is the aircraft analyzed in the present paper. The four-meter-span configuration contains four wing sections with span of 1.0 m and chord of 0.2 m each, as well as three pods at the connections between the wing panels. At the pods, the aircraft engines, landing gears, electronics and sensors are installed. Booms are connected to the pods and, at the tip of each boom, a horizontal tail is mounted. The two side tails are all-moving control surfaces that can be used for both longitudinal and lateral-directional control, and are then named as elevons. The central tail has a flipping-up capability, in order to modify the aircraft longitudinal and lateral-directional flying qualities as desired in operation. For ground clearance during take-off, the central tail has approximately 33% less span in its right (bottom) part than in the left (top) part. Anyway, all the configurations are analyzed in this paper with the central tail in the horizontal position. In all the configurations, the wing-tip sections have a dihedral angle of 10°. The wing is built with an incidence of 5°.

The 6m configuration has two more wing sections, two more pods, two more booms and two more tails than the 4m configuration. The 8m configuration has only two wing sections added with respect to the 6m configuration, without additional pods, booms or tails.

The numerical models consider the following stiffness properties for all the wing sections: $k_{11} = 2.14 \times 10^6$ N, $k_{13} = 1.54 \times 10^3$ N·m, $k_{14} = -4.91 \times 10^4$ N·m, $k_{22} = 55.8$ N·m^2, $k_{33} = 1.04 \times 10^2$ N·m^2, $k_{34} = -46.34$ N·m^2, and $k_{44} = 6.35 \times 10^3$ N·m^2. All the other aircraft components are assumed rigid.

The distributed mass properties of the aircraft components are shown in Table 1. The concentrated inertias match those listed in Table 7 of Ref. [2]. The three configurations' masses, CG locations, moments and products of inertia are shown in Table 2, in which the origin of the axes is located at the wing symmetry plane and at 28.8% of the wing chord. For the properties in Table 2, the x axis is directed rearward, y to the right semi-wing and z upward.

	Wing	Booms	Tails	Units
Elastic axis location (from L.E.)	28.8	-	32.35	% chord
CG location (from L.E.)	25.0	-	25.0	% chord
Mass per unit length	0.438	0.100	0.200	kg/m
I_{xx} per unit length	6.54×10^{-4}	2.91×10^{-5}	3.00×10^{-4}	kg·m^2/m
I_{yy} per unit length	1.34×10^{-2}	1.46×10^{-5}	1.50×10^{-4}	kg·m^2/m
I_{zz} per unit length	2.07×10^{-2}	1.46×10^{-5}	2.00×10^{-4}	kg·m^2/m

Table 1: Distributed mass properties of the aircraft components.

3.1 Verification of the models

Aircraft free-free or constrained modes of vibration (MOVs) can be calculated in both the formulation for small deformations and the geometrically-nonlinear formulation. In order to ensure that a fair basis for comparison of results between the formulations does indeed exist, it is fundamental that the modal frequencies predicted by both models satisfy some maximum difference tolerance.

First, then, for the 4m configuration, refined linear and nonlinear structural-dynamic models with 200 elements per wing section were generated. The first 40 constrained MOVs (with the

	4m	6m	8m	Units
x_{CG}	0.014	0.011	0.010	m
y_{CG}	-0.001	-0.001	-0.001	m
z_{CG}	-0.046	-0.052	-0.048	m
m	7.90	12.9	13.8	kg
I_{xx}^{CG}	6.51	28.5	39.3	kg·m^2
I_{yy}^{CG}	0.343	0.521	0.525	kg·m^2
I_{zz}^{CG}	6.79	29.0	39.8	kg·m^2
I_{xy}^{CG}	-0.0105	-0.0150	-0.0150	kg·m^2
I_{xz}^{CG}	0.0117	0.0209	0.0188	kg·m^2
I_{yz}^{CG}	-3.27×10^{-4}	-5.13×10^{-4}	-4.68×10^{-4}	kg·m^2

Table 2: Calculated mass properties for the three aircraft configurations.

clamp at the wing symmetry) were then calculated, and the maximum observed difference in frequency was 0.79% in a MOV above 200 Hz. The mesh with 800 elements in total was then held as the reference with which coarser meshes should be compared. Then, both structural-dynamic models were divided in much less elements per wing section.

The procedure showed that using only 10 elements per wing section in the geometrically-nonlinear formulation leads to errors in the constrained MOVs' frequencies of less than 4%, for modes up to 100 Hz, and less than 7.4%, for modes up to 200 Hz. In the model assuming small deformations, 20 elements result in errors less than 1.4%, for modes up to 100 Hz, and less than 2.6%, for modes up to 200 Hz. With such choices, the wing has the same quantity of nodes in both models.

The same discretization for each wing section was then adopted in the 6m and the 8m configurations. Free-free modes of vibration were then calculated for all the configurations. In all of them, the maximum difference in modal frequency predicted by the geometrically-nonlinear formulation when compared with the small-deformation one is less than 3.7% for modes up to 75 Hz. The natural frequencies of the free-free MOVs calculated with both formulations for all the configurations are shown in Fig. 1. From this point on, the implementation of the formulation for small deformations will have the acronym SDI, and the implementation of the geometrically-nonlinear formulation will have the acronym GNI.

The VLM mesh is the same for both formulations, and was, for simplicity, built to match the spanwise divisions of the wing sections in the nonlinear structural-dynamic model, that is, it comprises 10 uniformly distributed boxes spanwise per wing section. Chordwise, 8 boxes are used in the wing, also uniformly distributed. The tails are divided into 5 boxes chordwise and 6 boxes spanwise, except for the central tail, which has 33% less span in its right side and is divided in 3 boxes to the left side and 2 boxes to the right side. No effective vertical surface representing each pod is included in the aerodynamic model, also for simplicity.

The wing incidence of 5° and the wing reflexed EMX07 airfoil [2] camber are approximately represented by invariant normalwash vectors, given by the local effective camber line inclination at 75% of each box chord.

The VLM mesh is prepared to be updated in the formulation for large deformations, and its update is such that the boxes' side edges are displaced both laterally and vertically by exactly the same amount as the structural node with which they coincide spanwise (also valid for the

tails). Hence, the mesh update makes the aerodynamic forces consistently behave as follower forces in the geometrically-nonlinear formulation. The update can be easily disabled whenever desired.

The displacements and displacement rates of the beam elements' central nodes in the nonlinear formulation are directly used to calculate the normalwashes due to both the structural and the rigid-body motion. No camber deformation is considered, and hence the transferal of displacements and rates of displacements from the structural nodes to the boxes' control points is straightforward, assuming rigid arms. The aerodynamic loading is considered as distributed, and appropriate matrices transfer the distributed loads to nodal loads at each element.

On the other hand, the VLM mesh in the formulation for small deformations is never updated. Linear spline interpolation matrices, as derived in Ref. [15], are calculated and used. Differently from the geometrically-nonlinear implementation, the rigid-body aerodynamic contributions are previously calculated and summarized in classical coefficients and stability and control derivatives.

Both implementations allow the aircraft to be trimmed as if it were rigid. The results obtained for all configurations in steady turning flight with rate $\dot{\psi} = 30°/\text{s}$ at 14 m/s are shown in Table 3. The coincidence of the trimmed states and controls with two or three significant figures demonstrate that the aerodynamic model implemented in the GNI adequately recovers the forces and moments due to rigid-body motion and control surface deflection and, since exactly the same equations are used to calculate forces and moments due to elastic motion, the aerodynamic implementation can be considered validated.

The structural-dynamic models for small deformations and the VLM meshes are plotted in Figs. 2-4 for the three X-HALE configurations under analysis.

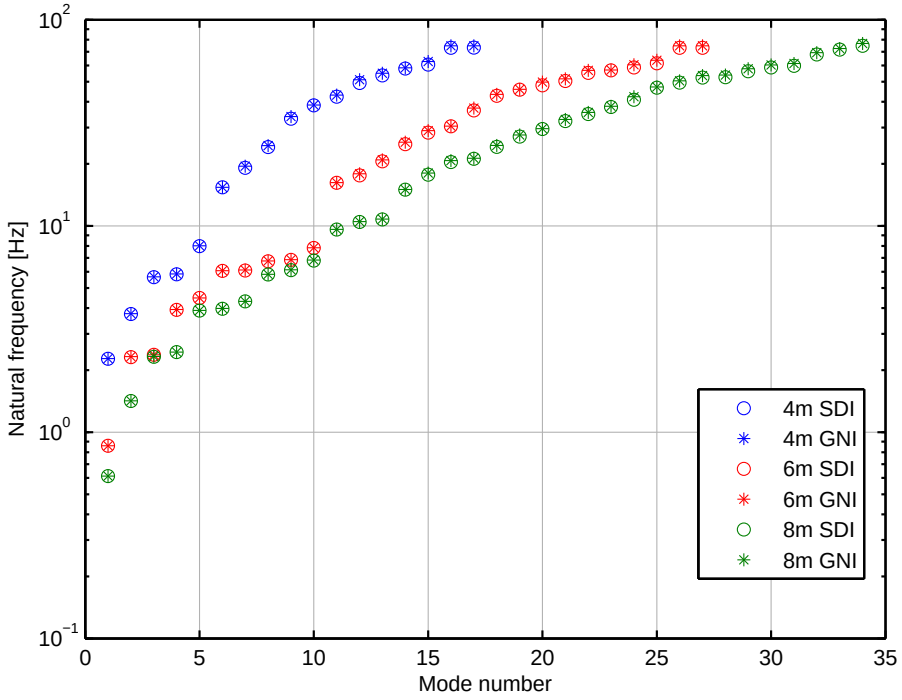

Figure 1: Natural frequencies of the free-free modes of vibration calculated with both the small-deformation and the geometrically-nonlinear implementation, for all three aircraft configurations.

	4m		6m		8m		
	SDI	GNI	SDI	GNI	SDI	GNI	Units
Angle of attack (α)	6.748	6.750	7.315	7.317	4.669	4.671	deg
Pitch rate (q)	17.93	17.93	17.92	17.92	17.93	17.93	deg/s
Bank angle (ϕ)	36.89	36.89	36.91	36.91	36.79	36.79	deg
Roll rate (p)	-2.827	-2.828	-3.063	-3.064	-1.958	-1.959	deg/s
Yaw rate (r)	23.89	23.89	23.86	23.86	23.97	23.97	deg/s
Left elevon(s) deflection	-7.446	-7.461	-8.016	-8.027	-6.297	-6.302	deg
Right elevon(s) deflection	-4.515	-4.530	-4.646	-4.656	-1.002	-1.007	deg
Left engine(s) thrust	1.628	1.629	1.408	1.408	1.498	1.499	N
Central engine thrust	1.517	1.517	1.268	1.269	1.371	1.371	N
Right engine(s) thrust	1.405	1.406	1.129	1.129	1.243	1.244	N

Table 3: Steady turning flight trimmed condition of the rigid aircraft with $\dot{\psi} = 30°/\text{s}$ at 14 m/s, calculated with both implementations for verification purpose.

Figure 2: Four-meter-span configuration SDI structural-dynamic model (left) and VLM mesh (right), as output from ITA/AeroFlex. Legend entries: GRIDs are the structural nodes; CBARNs are the beam elements; RBARs are rigid bar elements; CONM2 CGs are the CG locations of lumped-mass elements; and CONM2 Offsets are the offsets between such CG locations and the structural node the lumped-mass element is attached to. In the VLM model, control surfaces are plotted in orange.

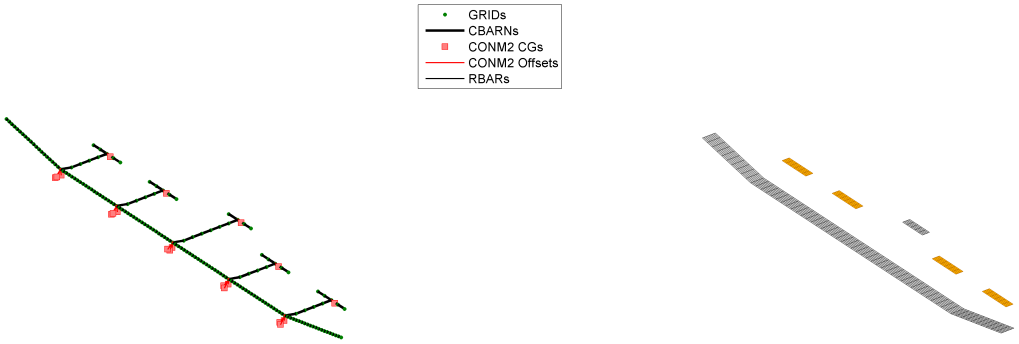

Figure 3: Six-meter-span configuration SDI structural-dynamic model (left) and VLM mesh (right), as output from ITA/AeroFlex.

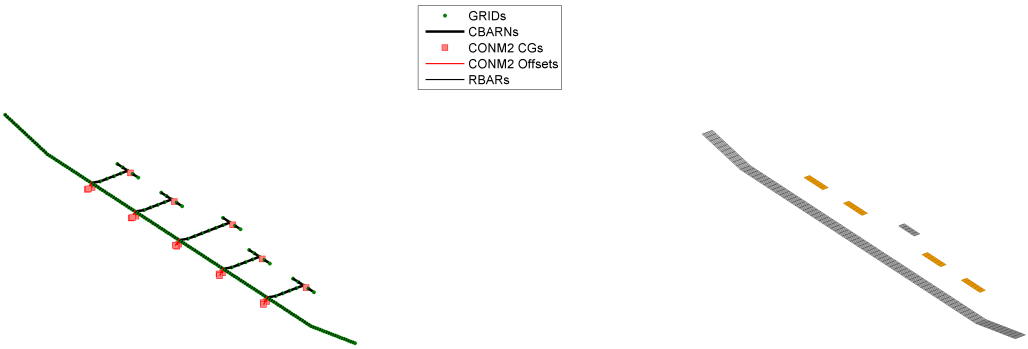

Figure 4: Eight-meter-span configuration SDI structural-dynamic model (left) and VLM mesh (right), as output from ITA/AeroFlex.

4 NUMERICAL RESULTS

In the results presented in this section, three different support locations (the support is the name of the point with null elastic displacements) are used in the formulation for small deformations. One is at a central location at the wing structural node in the wing symmetry plane, and is denoted by the acronym CTR. The two others are at the structural nodes at the wing tips, named LWT for the left one and RWT for the right one. Therefore, the plots that will be presented hereinafter will contain three data sets for the small-deformation implementation: SDI-CTR, SDI-LWT, and SDI-RWT. These shall be compared with the single data set obtained with the geometrically-nonlinear implementation, GNI.

In the determination of linearized dynamics about equilibrium conditions, stiffness-proportional structural damping is considered, with a constant of proportionality such that the first free-free mode of vibration presents 3% damping ratio.

4.1 Four-meter-span configuration

The four-meter-span configuration was trimmed in a variety of flight conditions at 14 m/s, 17 m/s and 20 m/s: level flight; steady turning flight with turn rates of 10°/s, 20°/s, and 30°/s; and longitudinal maneuver with nonzero pitch rate and vertical load factor of 2.0.

Figure 5 shows results for the trimmed level-flight condition. The difference between the different SDI support locations is very small, being more significant for the elevon deflections at 14 m/s. Thus, the proposed methodology predicts that the 4m configuration satisfies the assumption of small deformations. Indeed, comparison with the GNI results confirm that: the wing tip displacements are different between the linear and the nonlinear formulations only by millimeters.

The most critical of the flight conditions analyzed is that for a load factor of 2.0, the results of which are shown in Fig. 6. It is very interesting to see that dispersion exists between the SDI-CTR, SDI-LWT and SDI-RWT solutions, mainly in the control variables. This fact would imply that geometrical nonlinearities do potentially occur in this flight condition. Indeed, the results obtained with the GNI show greater wing tip displacements than the ones obtained with the SDI. The fact that the wing tip geometrically-nonlinear vertical displacements are around only 10% of the wing semi-span can be misleading as to whether the geometrical nonlinearity does in fact play an important role in the case.

It cannot be forgotten that the GNI considers not only a geometrically-nonlinear beam, but also a VLM mesh that has its panels' dihedral angles updated with the lifting surfaces' bending. With this, effective lift is lost due to the aerodynamic normal forces at the panels being follower forces, and the aircraft needs to be trimmed with higher angle of attack. Hence, the aerodynamic formulation plays a significant role in the nonlinearity of the flight-dynamic model. The deformation of the structure with load factor of 2.0 at 14 m/s is presented in Fig. 7.

The dynamics of the aircraft, represented by its equations of motion, can be linearized around an equilibrium condition, and the eigenvalues of the Jacobian matrix then provide information on the stability characteristics of the aircraft. Such linearization was then done around the level-flight condition, and Fig. 8 shows the obtained eigenvalues. An excellent correlation exists between the four different implementations, indicating that small disturbances around the level-flight condition are adequately captured with the formulation for small deformations.

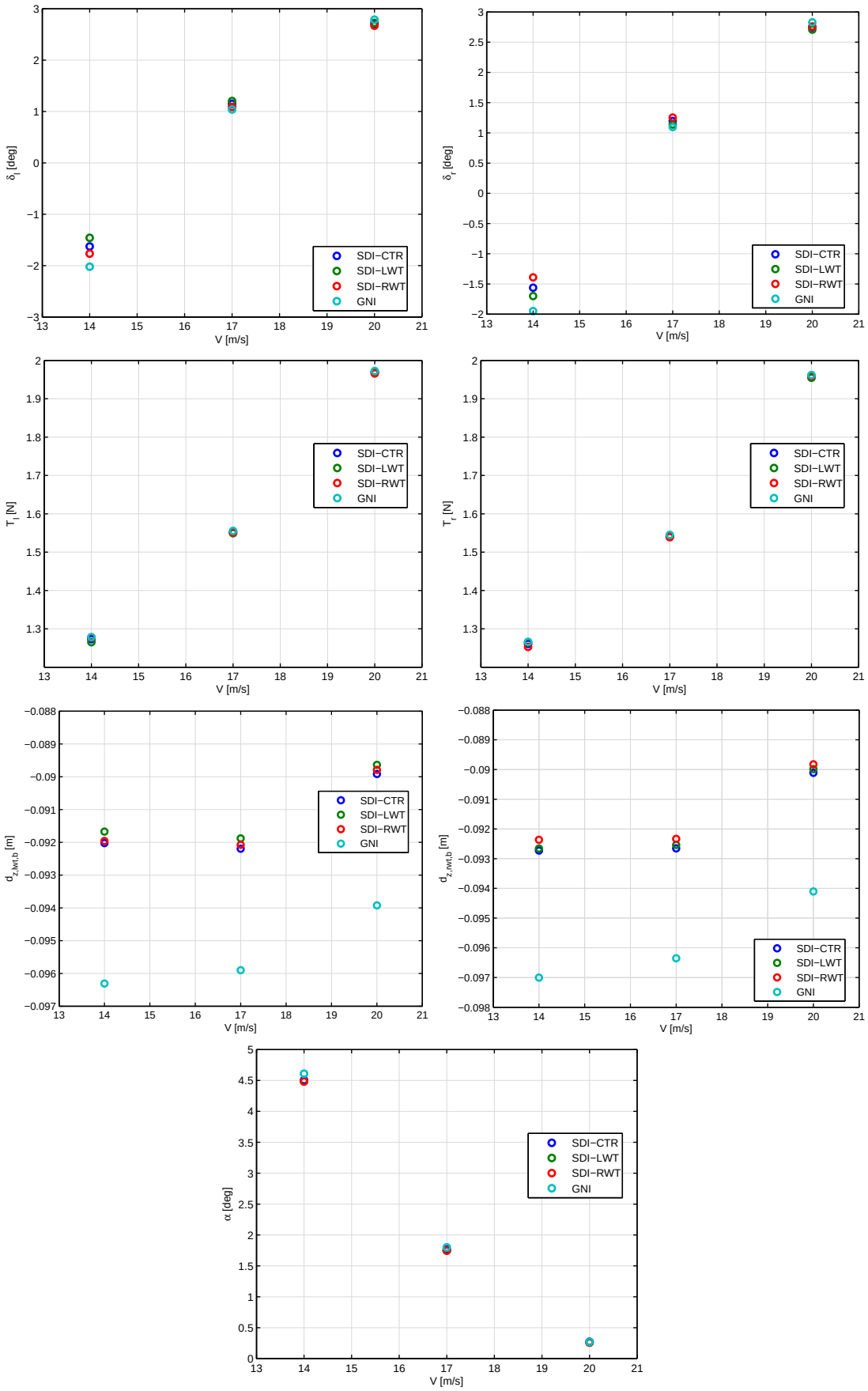

Figure 5: Trimmed level-flight condition of the four-meter-span configuration at different flight speeds.

4.2 Six-meter-span configuration

The six-meter-span configuration was trimmed in level flight and in steady turning flight with turn rate of 30°/s, at 14 m/s, 17 m/s and 20 m/s. Figure 9 shows results for the trimmed level-flight condition. The difference between the different SDI support locations is greater than in the 4m configuration, indicating a higher potential for nonlinearity, mainly at 14 m/s, where more significant dispersion in the control variables occurs. Indeed, comparison with the GNI results show that the wing tip displacements are different between the linear and the nonlinear formulations by up to 6 centimeters. The maximum wing tip displacement is about 11% of the wing semi-span, at 14 m/s.

In the steady turning flight condition, shown in Fig. 10, the dispersion between the SDI-CTR, SDI-LWT and SDI-RWT solutions is greater. The results obtained with the GNI show greater wing tip displacements than the ones obtained with the SDI. Vertical wing tip deflection of near 20% the wing semi-span is observed at 20 m/s. Once more, the aerodynamic mesh update is strongly related with the nonlinearity of the flight-dynamic model. The deformation of the structure in the steady turning flight at 20 m/s is presented in Fig. 11.

The linearized dynamics of the aircraft around the trimmed level-flight condition has a clear dispersion of the eigenvalues of the Jacobian matrix between the SDI-CTR and the SDI-LWT and SDI-RWT solutions, as seen in Fig. 12. It can be seen that mainly the damping is affected. The overall dynamic behavior is not expected to be accurately captured by the formulation for small deformations. If the structural damping had not be considered, several SDI-LWT and SDI-RWT would have become unstable.

The 6m configuration shall then be modeled preferably using the GNI, without which the risk of inaccuracies in the results increases.

4.3 Eight-meter-span configuration

Several test cases were planned for the eight-meter-span configuration, as for the other two configurations. However, a single case proved to be sufficient for a conclusion in this case. When trimming the 8m configuration in level flight at 14 m/s, the SDI-LWT and SDI-RWT failed to converge to a solution. Only the SDI-CTR (small-deformation implementation with a central support) was able to provide a valid trim condition.

On the other hand, the GNI (geometrically-nonlinear implementation) resulted in a valid trim condition with significant nonlinearities, as can be seen in Fig. 13. The wing tip vertical displacement is near 58% of the wing semi-span, and the magnitude of the displacement in y is about 1.2 m.

The failure of the wing tip supports in providing valid converged solutions to the trimming problem is therefore an irrefutable sign that strong geometrical nonlinearities occur, as confirmed by the U shape of the aircraft wing in this flight condition, a shape that cannot be achieved at all by a geometrically-linear formulation.

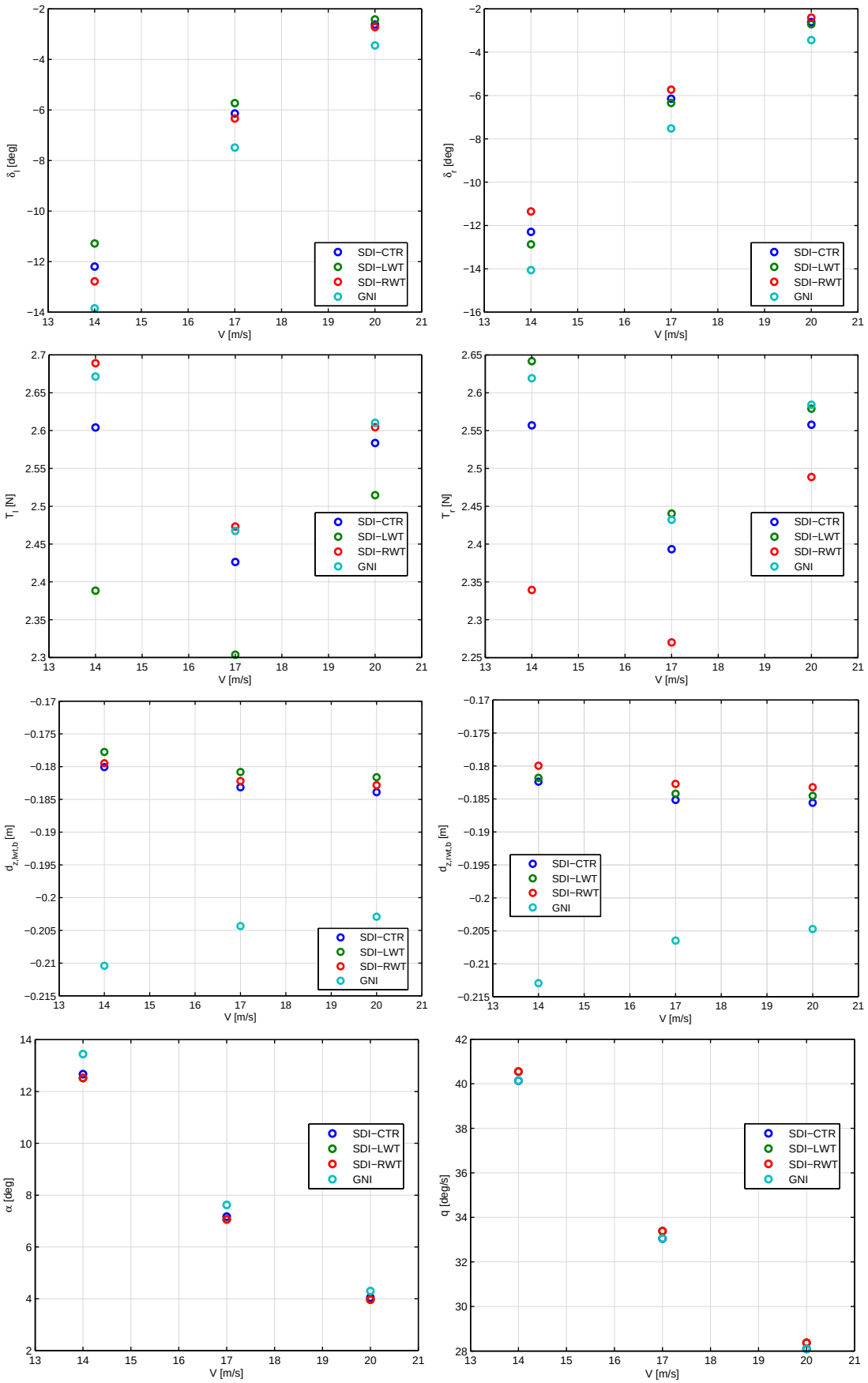

Figure 6: Maneuver of the four-meter-span configuration in the vertical plane with vertical load factor of 2.0, at different flight speeds.

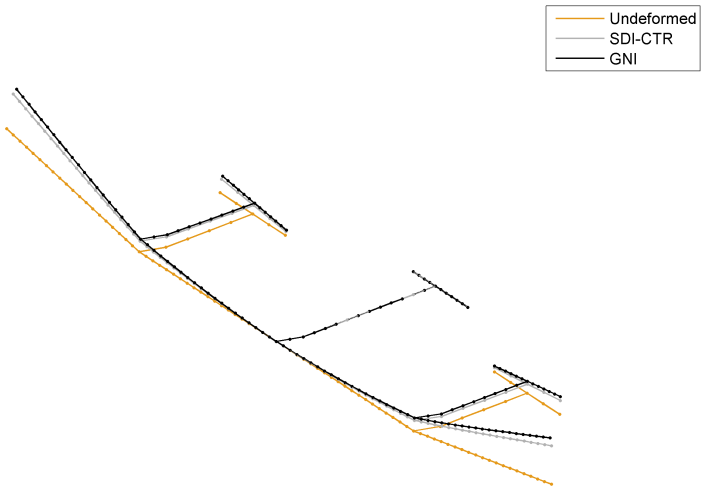

Figure 7: Deformation of the four-meter-span configuration with vertical load factor of 2.0, at 14 m/s.

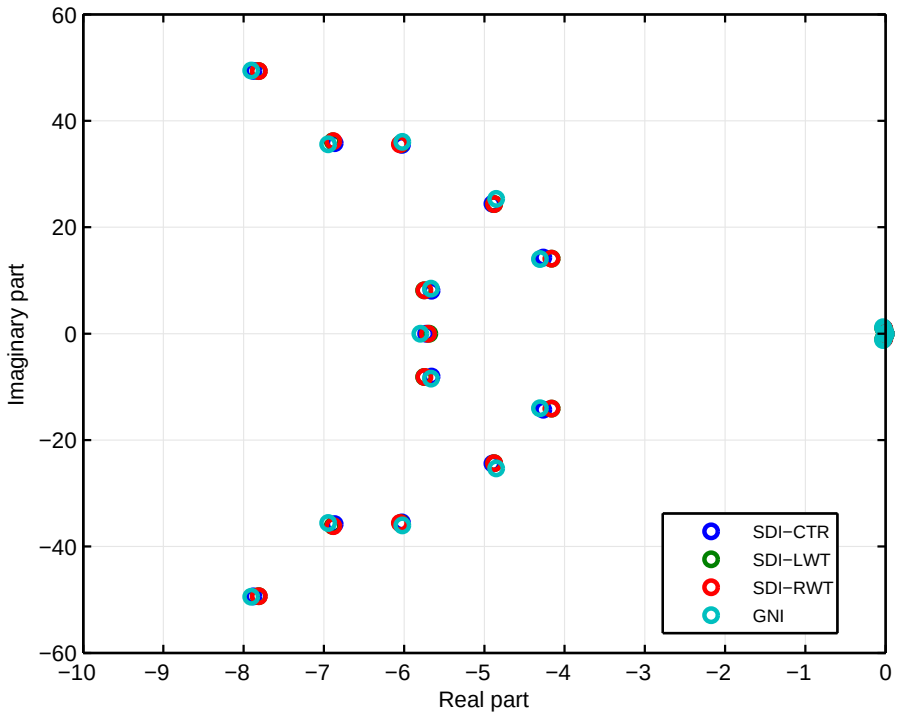

Figure 8: Low-frequency eigenvalues of the linearized dynamics of the four-meter-span configuration in level flight at 14 m/s.

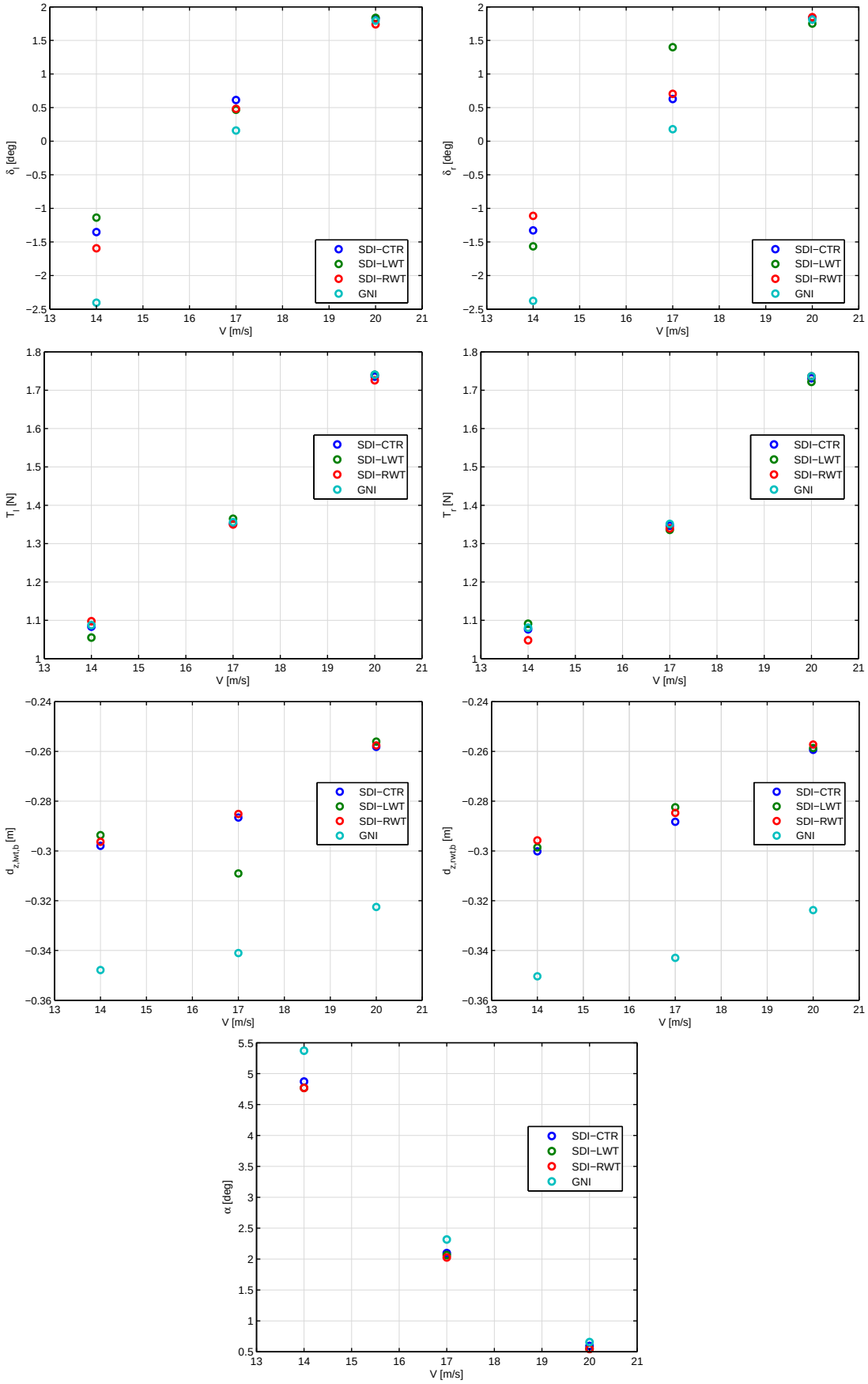

Figure 9: Trimmed level-flight condition of the six-meter-span configuration at different flight speeds.

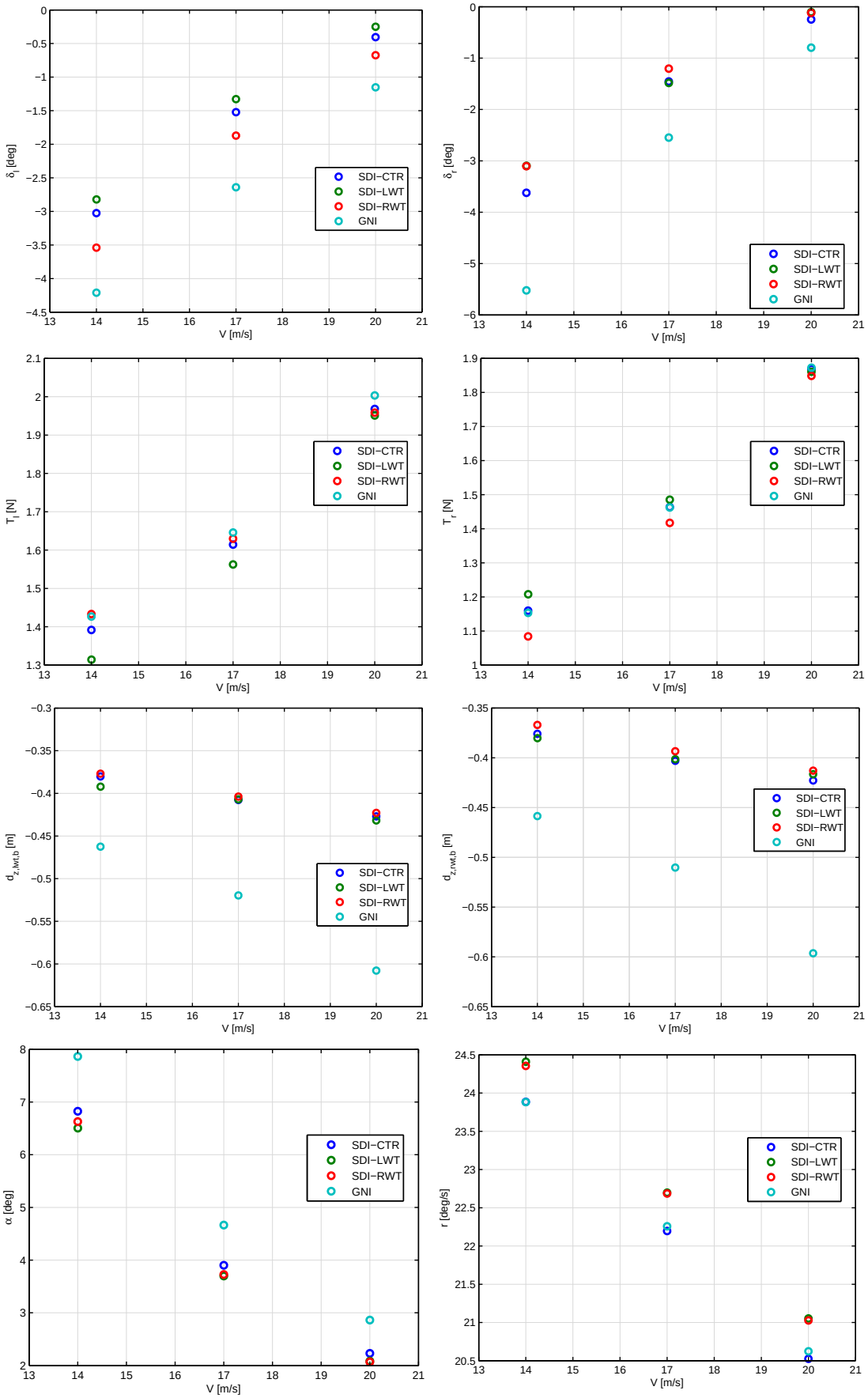

Figure 10: Steady turning flight condition with turn rate of 30°/s, for the six-meter-span configuration at different flight speeds.

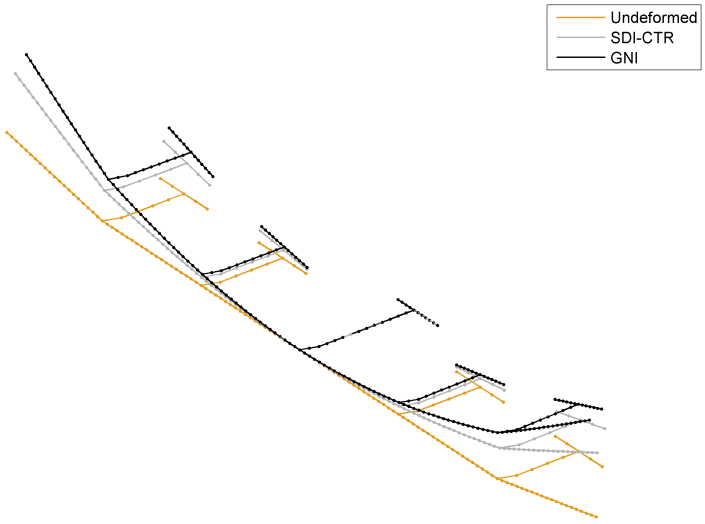

Figure 11: Deformation of the six-meter-span configuration in the steady turning flight condition with turn rate of 30°/s, at 20 m/s.

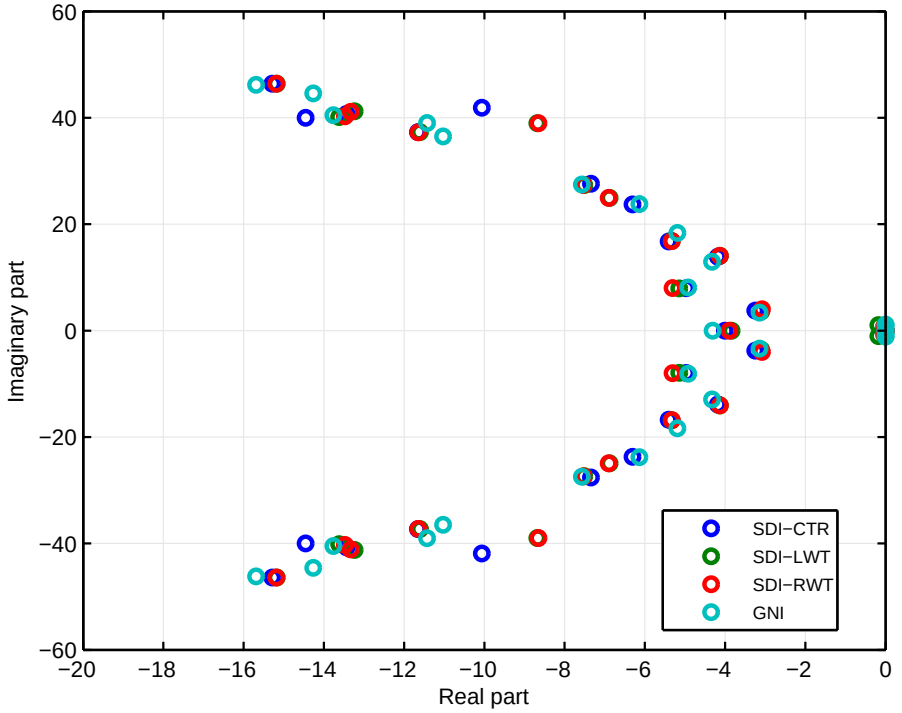

Figure 12: Low-frequency eigenvalues of the linearized dynamics of the six-meter-span configuration in level flight at 14 m/s.

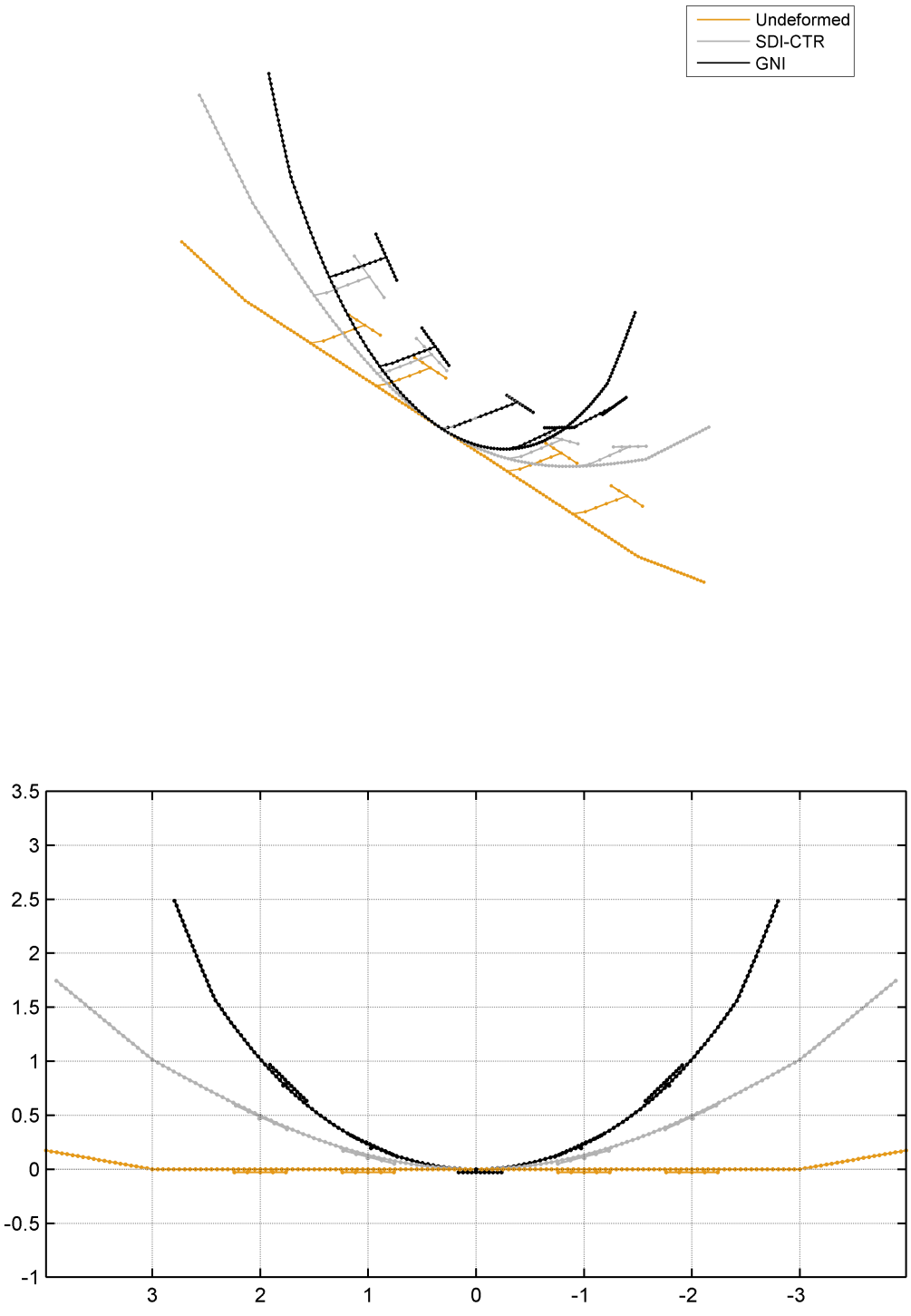

Figure 13: Deformation of the eight-meter-span configuration in the trimmed level flight condition at 14 m/s.

5 CONCLUDING REMARKS

A recently-proposed simple and self-contained methodology to assess the validity of the assumption of small deformations in structural-dynamic models was applied to aircraft with different levels of structural flexibility. The methodology does not depend on the availability of higher-fidelity, geometrically-nonlinear models, since it is based on the selection of two different structural nodes where the structural motion is to be, one at a time, completely constrained.

In order to validate the methodology, however, a geometrically-nonlinear model was necessary in this paper. Both the geometrically-linear and -nonlinear models were generated using the ITA/AeroFlex program, and several rigorous verifications were performed to ensure that both models satisfied the conditions to establish a fair basis for comparison of results, that is, the linearized structural dynamics of the geometrically-nonlinear model had to be close enough to the linear structural dynamics of the geometrically-linear implementation. Moreover, the same aerodynamic model should be employed. A quasisteady VLM was then used for both the linear and nonlinear implementations, with the difference that, in the latter, the VLM mesh was consistently updated with the structural deformation.

Results obtained for the free-free modes of vibration of the three different configurations of the X-HALE aircraft analyzed in this paper, as well as results for the rigid-body steady turning flight condition, showed that the small-deformation implementation and the geometrically-nonlinear implementation established a fair basis for comparison of results.

In the sequence, different steady-state flight conditions were analyzed. The four-meter-span configuration of the aircraft was seen to be accurately modeled using a geometrically-linear formulation, though less accurately at higher load factors. The dynamic modes of the linearized equations of motion did not alter significantly with different formulations.

For the six-meter-span configuration, greater differences were found in the control variables that trim the aircraft, mainly in a steady turning flight condition. A dispersion of the control variables by more than 10% can be taken as a criterion for establishing if a geometrically-nonlinear formulation would be beneficial.

The VLM mesh update was confirmed to be a source of nonlinearity that adds to the pure geometrical nonlinearity. Even with wing tip displacements less than 15% of the wing semi-span, significant differences occur between the small-deformation and the geometrically-nonlinear implementations. This nonlinearity comes from the fact that the aerodynamic normal forces at the VLM boxes become follower forces with the mesh update, and, as the deformation increases, less lift is generated by the geometrically-nonlinear formulation, implying the need for higher angles of attack.

Since there is a physical reason for the mesh update, this is clearly a disadvantage of the small-deformation implementation. It is also questionable whether including the aerodynamic mesh update in the geometrically-linear formulation would be worth the increased computing cost, as it seems that it would be wiser to exchange the whole formulation directly by the geometrically-nonlinear formulation.

For the eight-meter-span configuration of the X-HALE, the methodology proved its value in that it was not possible to obtain valid converged equilibrium solutions with the structural supports at the wing tips, only with the central support. A comparison with the geometrically-nonlinear

solution showed why this happened: the wing assumes a U shape in the trimmed level-flight condition, which is unachievable with a geometrically-linear formulation. Not being able to obtain equilibrium conditions with the wing tip supports in small deformations is then a definitive criterion for the use of geometrically-nonlinear formulations.

As seen, only steady-state flight conditions and linearized flight dynamics were analyzed in this paper. This work shall be extended to include general dynamic maneuvering conditions, in order to search for further limitations of the assumption of small deformations that are not yet transparent.

6 REFERENCES

[1] Guimarães Neto, A. B., Silva, R. G. A., Paglione, P., and Silvestre, F. J., "Formulation of the flight dynamics of flexible aircraft using general body axes," *AIAA Journal*, Vol. 54, No. 11, 2016, pp. 3516–3534. DOI: 10.2514/1.J054752.

[2] Cesnik, C. E. S., Senatore, P. J., Su, W., Atkins, E. M., and Shearer, C. M., "X-HALE: A Very Flexible Unmanned Aerial Vehicle for Nonlinear Aeroelastic Tests," *AIAA Journal*, Vol. 50, No. 12, 2012, pp. 2820–2833.

[3] Cesnik, C. E. S., and Brown, E. L., "Modeling of high aspect ratio active flexible wings for roll control," *Proceedings of the 43rd AIAA/ASME/ASCE/AHS/ASC Structures, Structural Dynamics, and materials conference and exhibit*, Denver, 2002. AIAA Paper 2002-1719.

[4] Cesnik, C. E. S., and Brown, E. L., "Active wing warping control of a joined-wing airplane configuration," *Proceedings of the 44th AIAA/ASME/ASCE/AHS/ASC Structures, Structural Dynamics, and materials conference and exhibit*, Norfolk, 2003. AIAA Paper 20031715.

[5] Shearer, C. M., and Cesnik, C. E. S., "Nonlinear flight dynamics of very flexible aircraft," *Journal of Aircraft*, Vol. 44, No. 5, 2007, pp. 1528–1545.

[6] Ribeiro, F. L. C., *Dinâmica de voo de aeronaves muito flexíveis*, Dissertation (MSc degree in Aeronautical and Mechanical Engineering), Instituto Tecnológico de Aeronáutica, So José dos Campos, Brazil, 2011.

[7] Bisplinghoff, R. L., Ashley, H., and Halfman, R. L., *Aeroelasticity*, Addison-Wesley Publishing Company, Inc., 1955.

[8] Bisplinghoff, R. L., and Ashley, H., *Principles of aeroelasticity*, Dover Publications, Inc., 1962.

[9] Etkin, B., *Dynamics of Flight Stability and Control*, John Wiley & Sons, Inc., 1959.

[10] Dusto, A. R., Brune, G. W., Dornfeld, G. M., Mercer, J. E., Pilet, S. C., Rubbert, P. E., Schwanz, R. C., Smutny, P., Tinoco, E. N., and Weber, J. A., "A method for predicting the stability characteristics of an elastic airplane: FLEXSTAB theoretical description," NASA-CR-114712., 1974 *apud* Abzug, M. J., and Larrabee, E. E., *Airplane stability and control:* a history of the technologies that made aviation possible, 2nd ed. Cambridge: University Press, 2002.

[11] Perkin, B. R., and Erickson, L. L., "FLEXSTAB - A Computer Program for the Prediction of Loads and Stability and Control of Flexible Aircraft," *Proceedings of the SCAR Conference*, Part 1, NASA CP-001, November, 1976.

[12] Milne, R. D., "Dynamics of the Derformable Aeroplane," Technical Report R&M 3345, Her Majestys Stationary Office, London, England, 1964.

[13] Lamb, H., *Higher Mechanics*, 2nd ed. Cambridge: University Press, 1929.

[14] Rodden, W. P., and Love, J. R., "Equations of Motion of a Quasisteady Flight Vehicle Utilizing Restrained Static Aeroelastic Characteristics," *Journal of Aircraft*, Vol. 22, No. 9, 1985, pp. 802-809.

[15] Rodden, W. P., and Johnson, E. H., *MSC.NASTRAN Aeroelastic Analysis User's Guide*, MacNeal-Schwendler Corporation, Los Angeles, 1994, Chap. 2.

[16] Dykman, J. R., and Rodden, W. P., "Structural Dynamics and Quasistatic Aeroelastic Equations of Motion," *Journal of Aircraft*, Vol. 37, No. 3, 2000, pp. 538–542.

[17] Waszak, M. R., and Schmidt, D. K., "Flight Dynamics of Aeroelastic Vehicles," *Journal of Aircraft*, Vol. 25, No. 6, 1988, pp. 563-571.

[18] Cavin III, R. K., and Dusto, A. R., "Hamilton's Principle: Finite-Element Methods and Flexible Body Dynamics," *AIAA Journal*, Vol. 15, No. 12, 1977, pp. 1684-1690.

[19] Buttrill, C. S., Zeiler, T. A., and Arbuckle, P. D., "Nonlinear Simulation of a Flexible Aircraft in Maneuvering Flight," *AIAA Flight Simulation Technologies Conference*, AIAA 87-2501, Monterey, California, Aug. 17-19, 1987.

[20] Zeiler, T. A., and Buttrill, C. S., "Dynamic Analysis of an Unrestrained, Rotating Structure through Nonlinear Simulation," *Structures, Structural Dynamics and Materials Conference*, AIAA-1988-2232, Apr. 18-20, 1988.

[21] Meirovitch, L., and Tuzcu, I., "Unified Theory for the Dynamics and Control of Maneuvering Flexible Aircraft," *AIAA Journal*, Vol. 42, No. 4, 2004, pp. 714-727.

[22] Meirovitch, L., *Methods of analytical dynamics*, Dover, Inc., 2003.

[23] Meirovitch, L., and Tuzcu, I., "Time simulations of the Response of Maneuvering Flexible Aircraft," *Journal of Guidance, Control and Dynamics*, Vol. 27, No. 5, 2004, pp. 814–828.

[24] Reschke, C., "Flight Loads Analysis with Inertially Coupled Equations of Motion," *AIAA Atmospheric Flight Mechanics Conference and Exhibit*, AIAA 2005-6026, San Francisco, California, Aug. 15-18, 2005.

[25] Reschke, C., *Integrated Flight Loads Modelling and Analysis for Flexible Transport Aircraft*, Dissertation for a Doctoral Degree, Institut Flugmechanik und Flugregelung der Universitat Stuttgart, 2006.

[26] Baldelli, D. H., Chen, P. C., and Panza, J., "Unified aeroelastic and flight dynamic formulation via rational function approximations," *Journal of Aircraft*, Vol. 43, No. 3, 2006, pp. 763–772.

[27] Mantegazza, P., "Tutorial on Attached-Mean Axes and Their Use in the Calculation of Deformable Static and Damped-Undamped Vibration Modes of a Free-Free Structure," *Journal of Aeroelasticity and Structural Dynamics*, Vol. 2, No. 1, 2011, pp. 81–98.

[28] Hesse, H., and Palacios, R., "Consistent structural linearisation in flexible-body dynamics with large rigid-body motion," *Computers & Structures*, Vol. 110-111, Nov. 2012, pp. 1–14. DOI: 10.1016/j.compstruc.2012.05.011.

[29] Brown, E. L., *Integrated strain actuation in aircraft with highly flexible composite wings*, Thesis (PhD) – Massachusetts Institute of Technology, 2003.

[30] Shearer, C. M., *Coupled nonlinear flight dynamics, aeroelasticity and control of very flexible aircraft*, Thesis (PhD in Aerospace Engineering) – University of Michigan, Ann Arbor, 2006.

[31] Su, W., *Coupled nonlinear aeroelasticity and flight dynamics of fully flexible aircraft*, Thesis (PhD in Aerospace Engineering) – University of Michigan, Ann Arbor, 2008.

[32] Su, W., and Cesnik, C. E. S., "Strain-based geometrically nonlinear beam formulation for modeling very flexible aircraft," *International Journal of Solids and Structures*, Vol. 48, No. 16-17, 2011, pp. 2349–2360. DOI: 10.1016/j.ijsolstr.2011.04.012.

[33] Cardoso-Ribeiro, F. L., Paglione, P., Silva, R. G. A., and Sousa, M. S., "AeroFlex : a toolbox for studying the flight dynamics of highly flexible airplanes," *VII Congresso Nacional de Engenharia Mecânica (CONEM)*, São Luís, Maranhão, Brazil, 2012.

[34] Noll, T. E. et al., *Investigation of the Helios prototype aircraft mishap*, Washington, DC: NASA, 2004.

[35] Patil, M. J., Hodges, D. H., and Cesnik, C. E. S., "Nonlinear aeroelastic analysis of complete aircraft in subsonic flow," *Journal of Aircraft*, Vol. 37, No. 5, 2000, pp. 753–760.

[36] Hodges, D. H., "A mixed variational formulation based on exact intrinsic equations for dynamics of moving beams," *International Journal of Solids and Structures*, Vol. 26, No. 11, 1990, pp. 1253–1273.

[37] Patil, M. J., Hodges, D. H., and Cesnik, C. E. S., "Nonlinear aeroelasticity and flight dynamics of high-altitude long-endurance aircraft," *Journal of Aircraft*, Vol. 38, No. 1, 2001, pp. 88–94.

[38] Cesnik, C. E. S., and Su, W., "Nonlinear aeroelastic modeling and analysis of fully flexible aircraft," *AIAA/ASME/ASCE/AHS/ASC 46th Structures, Structural Dynamics and Materials Conference*, 2005, Austin. AIAA Paper 20052169.

[39] Stevens, B. L., and Lewis, F. L., *Aircraft control and simulation*, Wiley, Hoboken, NJ, 2003, pp. 25–29; 116–138; 263–265.

[40] Bismarck-Nasr, M. N., *Structural Dynamics in Aeronautical Engineering*, AIAA Education Series, AIAA, Reston, VA, 1999, pp. 53–91.

[41] Hedman, S. G., "Vortex Lattice Method for Calculation of Quasi Steady State Loadings on Thin Elastic Wings," Aeronautical Research Inst. of Sweden Rept. 105, Stockholm, 1965.

[42] Albano, E., and Rodden, W. P., "A doublet-lattice method for calculating lift distributions on oscillating surfaces in subsonic flows," *AIAA Journal*, Vol. 7, No. 2, 1969, pp. 279–285, DOI: 10.2514/3.5086.

[43] Craig Jr., R. R., and Kurdila, A. J., *Fundamentals of structural dynamics*, Wiley, Hoboken, NJ, 2006, pp. 539–544.

[44] Przemieniecki, J. S., *Theory of Matrix Structural Analysis*, McGrawHill, New York, 1968, pp. 129-148.

[45] Guimarães Neto, A. B., *Flight dynamics of flexible aircraft using general body axes: a theoretical and computational study*, Thesis (PhD in Aeronautical and Mechanical Engineering) – Instituto Tecnológico de Aeronáutica, São José dos Campos, Brazil, 2014.

[46] Giesing, J. P., Klmn, T. P., and Rodden, W. P., *Correction factor techniques for improving aerodynamic prediction methods*, NASA-CR-144967, 1976.

[47] Silva, R. G. A., Mello, O. A. F., Azevedo, J. L. F., Chen, P. C., and Liu, D. D., "Investigation on transonic correction methods for unsteady aerodynamics and aeroelastic analyses," *Journal of Aircraft*, Vol. 45, No. 6, 2008, pp. 1890–1903. DOI: 10.2514/1.33406.

[48] Guimarães Neto, A. B., Silva, R. G. A., and Paglione, P., "Control-point-placement method for the aerodynamic correction of the vortex-and the doublet-lattice methods," *Aerospace Science and Technology*, Vol. 37, 2014, pp. 117–129. DOI: 10.1016/j.ast.2014.05.007.

[49] Eversman, W., and Tewari, A., "Consistent rational function approximation for unsteady aerodynamics," *Journal of Aircraft*, Vol. 29, No. 9, 1991, pp. 545–552.

[50] Roger, K. L., *Airplane math modeling methods for active control design*, AGARD-CP-228, 1977.

[51] Kálmán, T. P., Giesing, J. P., and Rodden, W. P, "Spanwise distribution of induced drag in subsonic flow by the vortex lattice method," *Journal of Aircraft*, Vol. 7, No. 6, 1970, pp. 574–576.

COPYRIGHT STATEMENT